Faculty of Automation and Computers

Master Program: Information Technology

Study of UV-C Intensity Distribution Using the TIAMO-C6 Sensor

Dissertation Thesis

Scientific Coordinator,
Assoc. Prof. Dr. Ing. **Raul IONEL**

Graduate,
Nicu-Şerban POP

Timişoara,
2021

Contents

List of Figures

List of Tables

1. Introduction

Ultraviolet radiation exists everywhere around us in our life with the except of UV-C and lower wavelength light. UV light is part of the electromagnetic spectrum with a wavelength ranging from 100nm to 400nm[1]. The wavelength range in UV disinfection that we are going to work on is 220-280nm (UV-C), specifically 253.7nm, bacteria having the highest light absorbance from 250nm to 265nm.

Biological effects in human's overexposure to UV-C radiation varies with wavelength, photon energy and duration of exposure[2]. UV-C is classified as probable human carcinogen by the US National Toxicology Program with various consequences depending on exposure time, ranging from mild rashes especially in the eye region and in some cases may even lead to skin cancer and death.

Ultraviolet light is invisible to the naked human eye and is classified into four parts as seen in Figure 1-1: UV-A (315nm – 400nm), UV-B (280nm-315nm), UV-C (200nm-280nm) and vacuum UV (100-200nm).
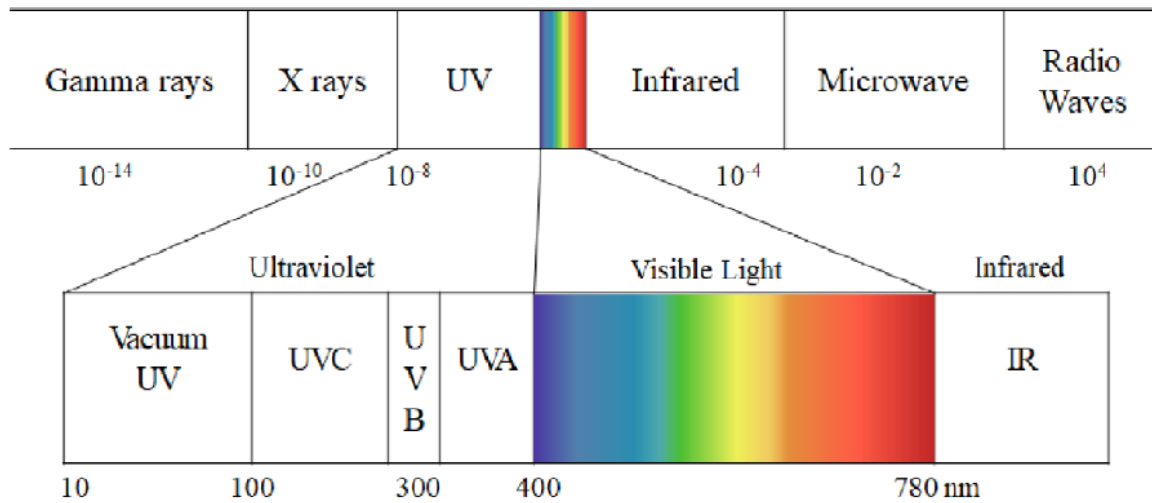
Figure 1-1. Light wavelength, taken from [3]

Ultraviolet disinfection is one method of disinfection that has been widely used in equipment sterilization using germicidal UV-C (254nm). Germicidal action is maximized at 265nm and decreases linearly over and under said value. At 254nm we achieve an efficiency of approximate 85% for a low-pressure lamp as the one used in our tests as illustrated in Figure 1-2 taken from [4].
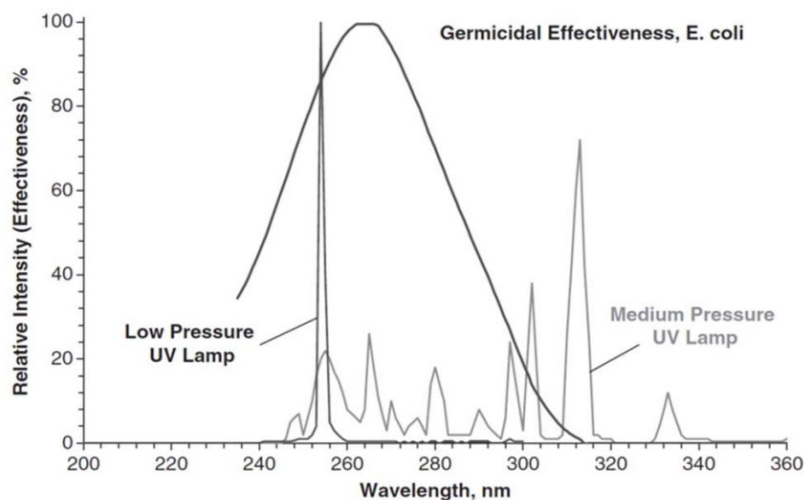
Figure 1-2. UV-C wavelength

Modern UV disinfection technologies have good disinfection efficiencies against bacteria and viruses and poses little to no formation of disinfection by-products [5]. Ozone that is produced by mercury-lamp UV lamps is also an effective disinfectant, particularly against viruses but poses concerning health issues, specifically formation of bromate that is a suspected human carcinogen [6].

UV disinfection is achieved by exposing pathogens (viruses, bacteria, spores and other microorganisms) to UV radiation. The UV radiation penetrates the wall of the microorganisms and changes the photochemical structure of said pathogens killing them [7].

When the emitted ozone is exposed to the UV light from the lamp, hydroxyl radical is produced through photolysis and is usually classified as Advanced Oxidation Process [8].

Taking all of this into consideration we are left with the conclusion that is not safe for human beings to be present in the same location as a running UV light but also after the use of it.

We aim to demonstrate UV-C radiation losses and efficiency over various distances without human interaction. The proposed platform shall move in the desired area, identify and measure the 253.7nm radiation, if any, produced by various sources. The platform is remote-controlled from a safe distance and can measure the intensity of a single point in a short period of time or produce a 2D matrix representing the UV-C radiation over a longer period of time. Ultraviolet disinfection is one method of the disinfection that has been widely used in equipment sterilization using germicidal UV-C (**254nm**).

Following we'll introduce a robotic platform that can be remotely operated and sent into an area with presence of ultraviolet radiations without the operator needing to expose himself to said radiations and can detect and measure light radiations of type UV-C.

2. State of the art

Ultraviolet (UV) irradiation, due to the germicidal properties, is a widely used and effective noncontact method for inactivating viral pathogens. In many applications, such as ground, surface, or water sterilization, it is accepted as an attractive and cost-effective means for pathogens control. Over the last decade, but specially in the context of the SARS-CoV-2 pandemic, numerous types of UV generating devices have been developed and are commercially available. These "no-touch" technologies, like aerosol and vaporized hydrogen peroxide spreading devices, UV emitting devices, pulsed-xenon UV light systems etc., have proven to be capable to reduce bacterial contamination. However, continued efforts to improve manual decontamination methods are justified

Research activities analyzing the efficiency of modern technologies used to supplement traditional cleaning and disinfection methods, have become increasingly popular [9-11].

Pathogens disinfection by using ultraviolet radiation, also known as ultraviolet germicidal irradiation (UVGI) is used in disinfecting water, air, food etc. and has been used since the 20th century. In the early years of the 20th century, France used UV-C disinfection techniques since 1908 to disinfect water supply in its cities. After 1950s, UVGI started to be adopted in sterilizing air in hospitals, storage facilities, kitchens, pharmaceutical plants and so on. Ultraviolet radiation in the range 225-302nm is lethal to microorganisms and is referred to as ultraviolet germicidal irradiation, or UVGI [12]. The microorganism's population is described by the exponential decay equation (2-1) where $S(t)$ is the population fraction at time t, k_0 is the overall decay rate constant (s^{-1}) and t is the time in seconds.

$$S(t) = e^{-k_0 t} \tag{2-1}$$

The overall decay rate constant k_0 also defines the sensitivity of the microorganism and is unique to each microbial species. The decay rate linearly increases as a function of the UVGI irradiation as can be seen in Figure 2-1 where I is the intensity of UVGI irradiation measured in µW/cm².
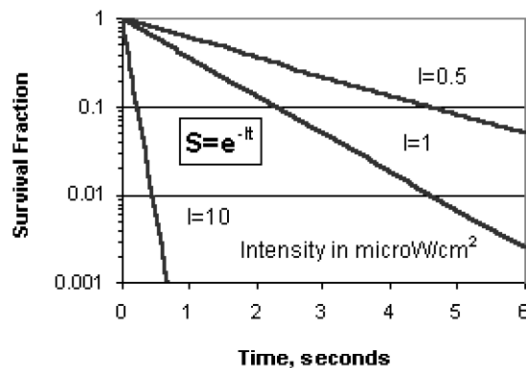
Figure 2-1. Microorganism survival rate based on irradiation intensity, taken from [12]

We can deduct from this that the higher the intensity of the UVGI irradiation (a.i. higher µW/cm²) the lower the survival rate of the microorganism.

UV-C radiation is weak in nature, the ozone layer of the Earth's atmosphere blocks it [13]. In order to have sustainable UV-C sterilization on our planet we need UVGI devices that can produce said UV-C radiation.

In present day, UV disinfection is done mostly by mercury-vapor lamp. Low-pressure mercury-vapor emits at approximately 254nm which is close to the optimal wavelength of disinfection (260-265nm). A typical low-pressure, mercury vapor lamp has an efficiency of approximately 35% of UV-C light, with the rest of 65% made up of different wavelengths such as visible light [14].

More recent development in LED technology have led to commercially available UV-C LEDs which allows the creation of small and portable devices for disinfection [15]. UV-C LEDs don't have a longer lifetime in terms of hours used, but have more variable characteristics than mercury lamps with a better tolerance for short-term operations.

3. Overview

In order to remotely detect and measure ultraviolet radiations without getting exposed to the UV radiations, a moving platform with sensors is to be created as follows.

The platform is able to move in all directions, forward/backward, left/right but also diagonally with the ability to rotate in place. This configuration was chosen in order to allow the platform to be easily moved inside different rooms and overcome/avoid obstacles.

The sensor that we are using together with a video camera is attached to the platform's head. The head is made up of two servomotors in order to give the head 2-directional movement (up/down, left/right). This configuration allows for the user to individually control the camera mounted on two axes with the moving head without moving the actual platform and allows for a 2-dimensional matrix to be produced.

The platform can be controlled over Bluetooth with a PS4 Controller shown in Figure 3-1.a or over wireless with a MC6C remote controller transmitter from MicroZone shown in Figure 3-1.b.

Figure 3-1. a PlayStation 4 DualShock 4 Controller   Figure 3-1. b MC6C RC Transmitter

The platform can also be controlled through the original remote controller with a few minor adjustments to the system. It is not very accurate, it not having an analog joystick but only digital buttons for control that we are not going to use.

The system needs two power sources in order to function properly. One power-bank for powering the control circuits that include the Raspberry Pi, the Arduino Nano, cameras, ESP32, radio receiver at a constant voltage of 5V. The system also requires a set of batteries ranging from 5V to 50V, 7.4V in our case, for powering the driving motors and servo motors.

The system can be controlled from up to 8-10 meters with the DualShock controller and up to 1000 meters with the MC6C controller, with obstacles such as walls and buildings or other radio interferences significantly decreasing said distance.

In Figure 3.2 is presented a general overview of the platform to be implemented, consisting of a Raspberry Pi 4 acting as the master controller, an Arduino Nano for reading analog sensor data, a camera connected to the RP4 and the six motors, two servo motors for moving the head and four DC motors for driving the wheels.
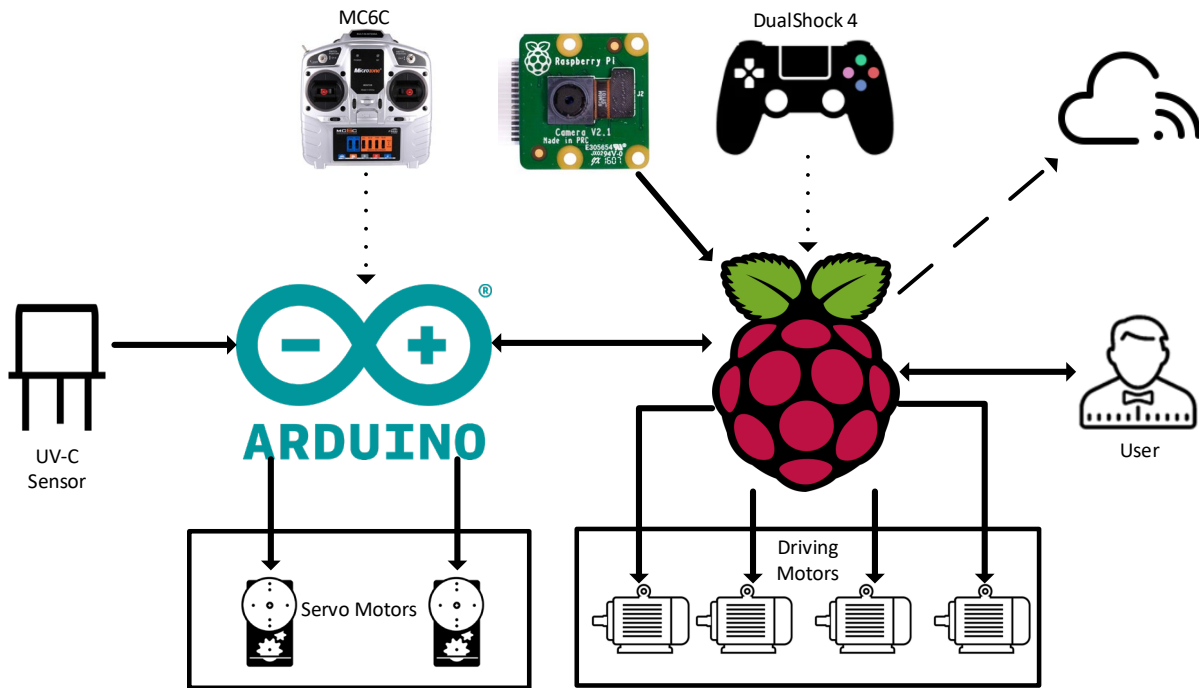
Figure 3.2 System Overview

Implementing everything from the sketch we get the results shown in Figure 3.3.
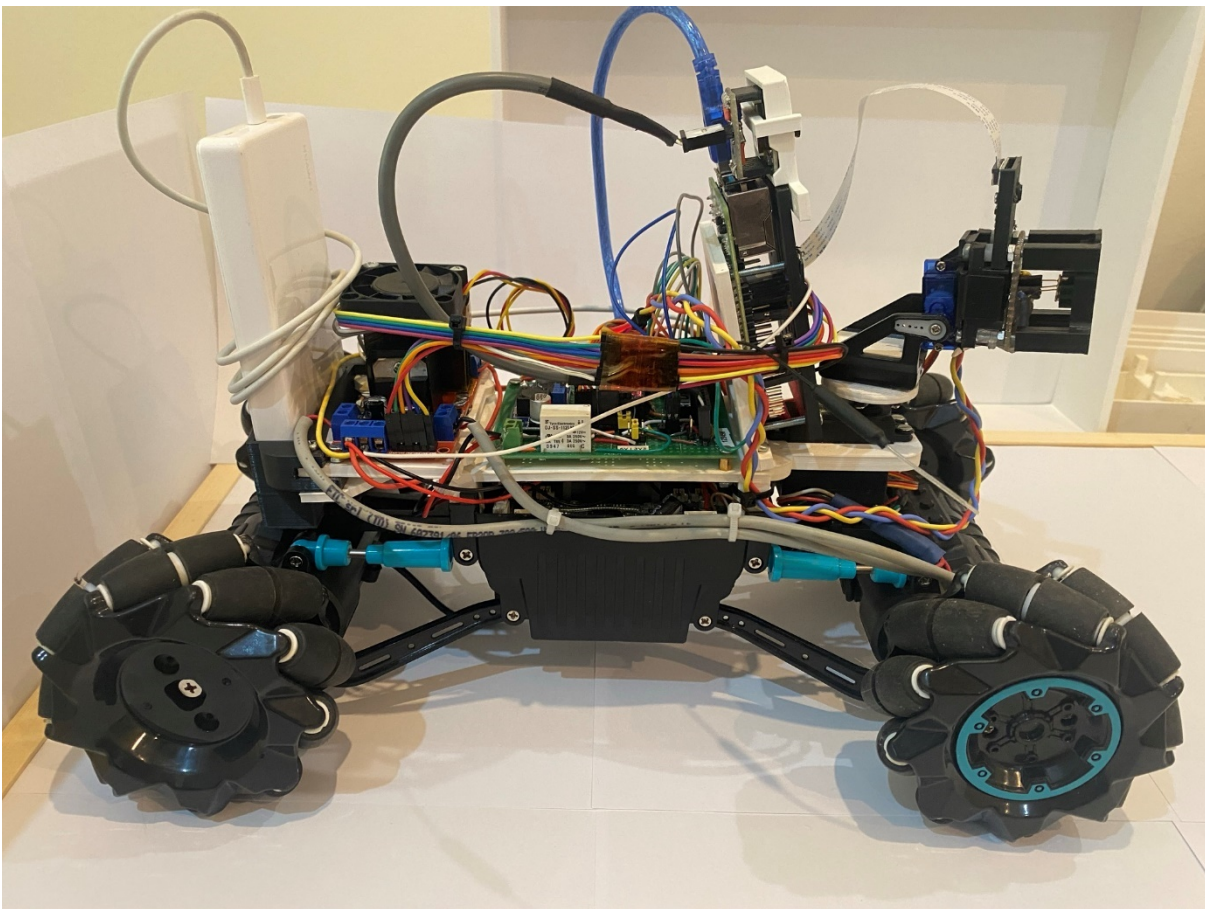
Figure 3.3 Finished Platform Prototype

4. Architecture

The platform is a heavily modified version of the remote-controlled car iDrive Rock Climber shown in Figure 4-1. The RC car was stripped of almost all features leaving only the base chassis and the four engines with wheels.

Figure 4-1. iDrive Rock Climber RC Car

The platform has a single 9V battery for powering only the motors for an autonomy of approximately 7 minutes and a double 3.7 Li-Ion battery pack for a total of 7.4V capable of powering the platform for about 22 minutes. Said batteries only power the 4 driving motors and the two servo motors attached to the sensors.

The DualShock 4 controller's UART is based on the Qualcomm Atheros AR3002 single chip with Bluetooth 4.0 and is capable of communications at a baud rate of exactly 3Mbit/s [16] and adheres to the HCI standards (8N1). The report rate ranges from once every 1.3 milliseconds in normal operation to 15 milliseconds when certain gaps occur.

The MC6C controller communicates over standard wireless over a frequency of 2401.5MHz−2445.5MHz with a power up to 100mW. This controller also needs the MC6RE receiver shown in Figure 4-2 in order to communicate with devices. This receiver operates on the same frequency as the transmitter (2401.5MHz-2445.5MHz) and has a sensitivity of -97dBm [17].

Figure 4-2. MC6RE 6-channel receiver

Due to the fact that the communication between the transmitter (MC6C) and the receiver (MC6RE) is done through the same frequency as conventional wireless routers (2.4GHz) the risk of interference is high. In order to fix this problem, a modulation scheme is required. Both devices use the frequency-hopping spread spectrum (FHSS) modulation scheme in which the radio signal occupies a larger spectral band than a fixed-frequency transmission.

4.1. Hardware Architecture

The entire system is managed by a Raspberry Pi 4 that controls the platform movement, provides a video stream to the user and can also compute the results on the spot.

The sensor we are using to measure light radiation is the UV-TIAMO-C6 which is a UV-C only amplified SiC UV detector. It operates in the range of 225-287nm with a max irradiance of $1.8mW/cm^2@254nm$. From [18] we can see in Figure 4-3. the spectral responsivity of the sensor. It can be noted that the sensor is most efficient at 275nm wavelength but we achieve a spectral responsivity of around 70% at a wavelength of 253.7nm.
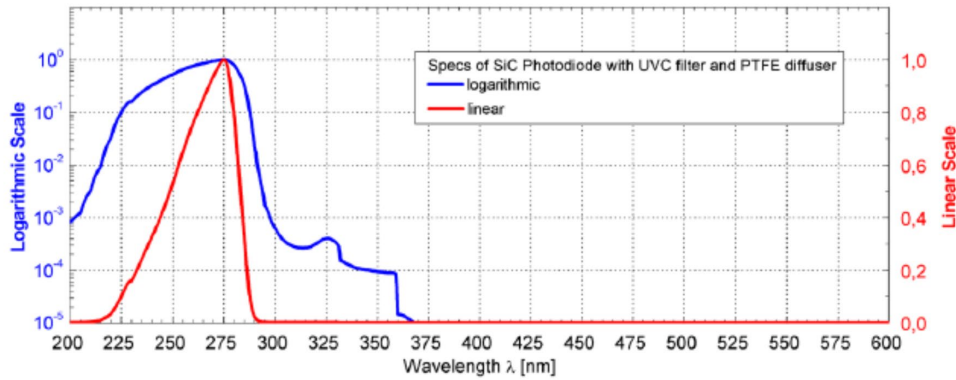
Figure 4-3. UV-TIAMO-C6 Normalized Spectral Responsivity

The responsivity of the UV sensor is the ratio of generated photocurrent and incident optical power determined in the linear region of response [19].

The UV sensor is an analog sensor and in order to be able to read it with the Raspberry Pi which only has digital inputs, we need an analog-to-digital (ADC) converter. We are using an Arduino Nano with a resolution of 10 bits ADC for this purpose. The Arduino Nano is also responsible for driving the servo motors.

The entire circuit diagram of the system is illustrated in Figure 4-4. For driving motors that require large amounts of power, two L298N dual full-bridge drivers are used. Each driver is capable of bi-directionally driving two sets of motors of up to 50V/3A and are powered directly from the platform's battery pack, while control is done through the Raspberry Pi.
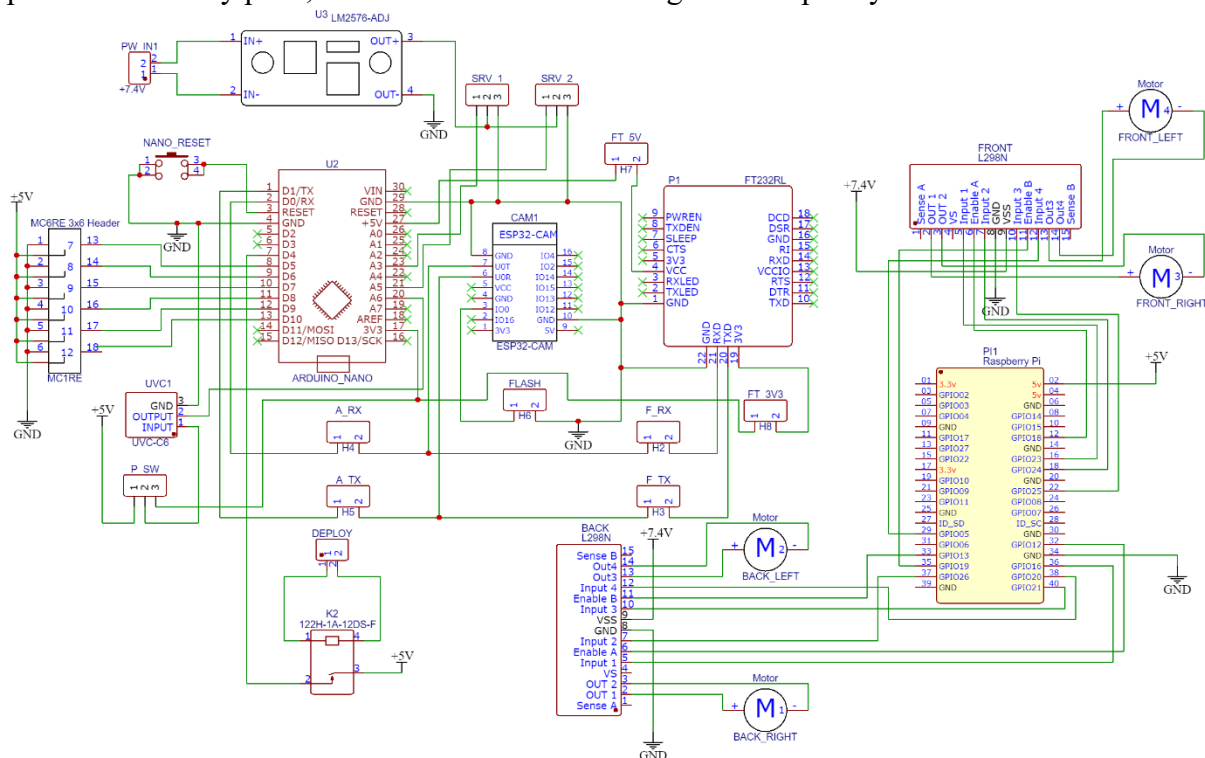
Figure 4-4. System Circuit Diagram

The system requires +5V for it to work properly and is provided by an external power bank. The servo motors attached to the head draw too much power if connected directly to the same power source as the rest of the system and problems such as: loss of wireless communication, video problems, sensor inaccuracy arise. Because of this, the servos that require +5V to operate will draw power directly from the platform's battery pack (the same source used for driving motors) through a LM2576 step-down converter as shown in Figure 4-5 in order to provide a stable 5 volts supply. The LM2576 regulator is

14

able to produce a steady voltage ranging from 3.3V up to 15V [20]. The output voltage is adjusted by using the on-board potentiometer.

Figure 4-5. LM2596S Step down converter

The system can also be operated without the use of a Raspberry Pi, through an ESP32, specifically an ESP32-CAM with minor adjustments. The ESP32 has a microcontroller instead of a processor like the one provided by the Raspberry Pi but it is still capable of providing a video feed at a lower resolution (1280x1024 vs 3280x2464) and it needs to have an internet connection in order to function properly.

4.2. Software Architecture

From a software perspective, the system uses a multitude of libraries and server such as a python server where everything is centralized containing the *PiCamera* python library for the video streaming server, the *gpiozero* library used for controlling the L298N motor drivers, the *ESP32 Camera Driver* library for controlling the ESP32 and the Processing software on the RP4 for generating the matrix images. The software layout is shown in Figure 4-6. For controlling the platform, a python server has been made. It is responsible for communication between the Raspberry Pi, either through Bluetooth or through wireless, for controlling the motors, sending video feed to the web server in order for the user to see the video stream and running the Arduino program which is responsible for driving the servo motors attached to the head and reading the UV sensors.
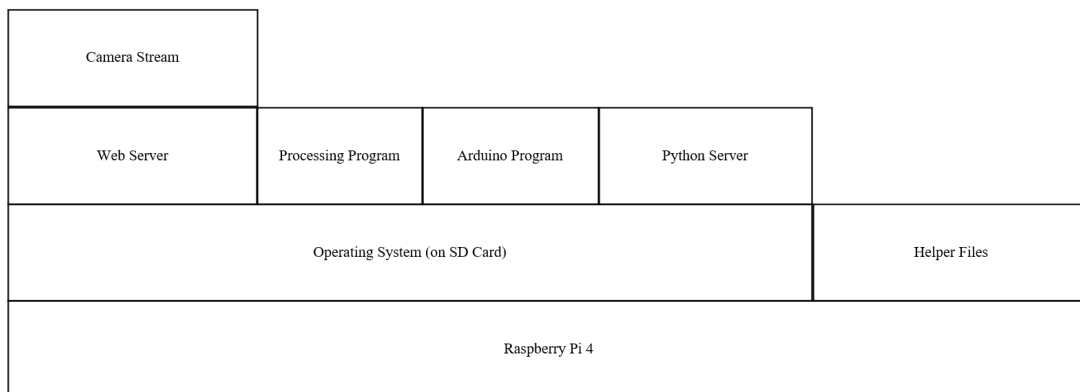
Figure 4-6. Raspberry Pi Software Layout

In order for the system to be able to produce the 2-dimensional matrix mentioned earlier, a predetermined path must be created. This path is similar to a matrix traversal and is illustrated in the table below in Figure 4-6, each number represents the current step in reading.

1	2	3	4	5	6	7	8	…	100
200	199	198	197	196	195	194	193	…	101
201	202	203	204	205	206	207	208	…	300
400	399	398	397	396	395	394	393	…	301
…	…	…	…	…	…	…	…	…	…
5501	5502	5503	5504	5505	5506	5507	5508	…	5600

Figure 4-7. 100x56 Sensor Path

The path starts at the upper left-most point and goes horizontally to the right-most point (left to right). Once this point has been reached, a line-reading has been completed and is sent from the Arduino to the Raspberry Pi for processing. This is done because the Arduino will not fit the entire matrix in its memory, the matrix can take up to 89.6Kb while the Arduino Nano has only 32Kb and parts of it are needed for operating the Arduino, store variables, functions etc. At this point, the same procedure is repeated in reverse order (right to left) after taking a vertical servo step (up-down).

The matrix has the dimensions of 100x56 in order to allow an angle of 90° angle between the sensor and the horizontal line reading plus an eventual 5% of error on both sides. Vertically, it has 56 passes in order to keep the same aspect ratio as the camera mounted on its head (16:9). This can be modified if the ESP32 is used instead of the Raspberry Pi, with a new aspect ratio of 4:3.

5. Implementation

5.1. Hardware Implementation

The base model of the platform has been created using 3D printed parts. In Figure 5-1 is illustrated the base for the platform. It consists of a flat base for circuits, a power bank support for the battery that is going to power the system and the moving head made up of two servo motors, a video camera for video streaming and taking pictures, the UV-TIAMO-C6 UV sensor and its protective housing.
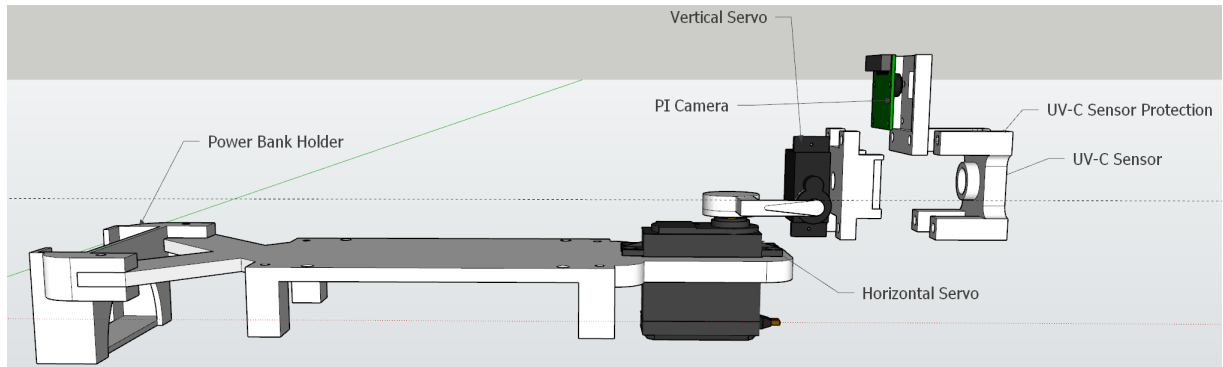
Figure 5-1. 3D Base Components

5.1.1. Moving Head

The 2D matrix is created by moving the sensor head in two directions, as shown in Figure 5-2. The head is able to be moved up and down, left and right either by using one of the remote controllers or by starting the measuring cycle for 2D matrix.
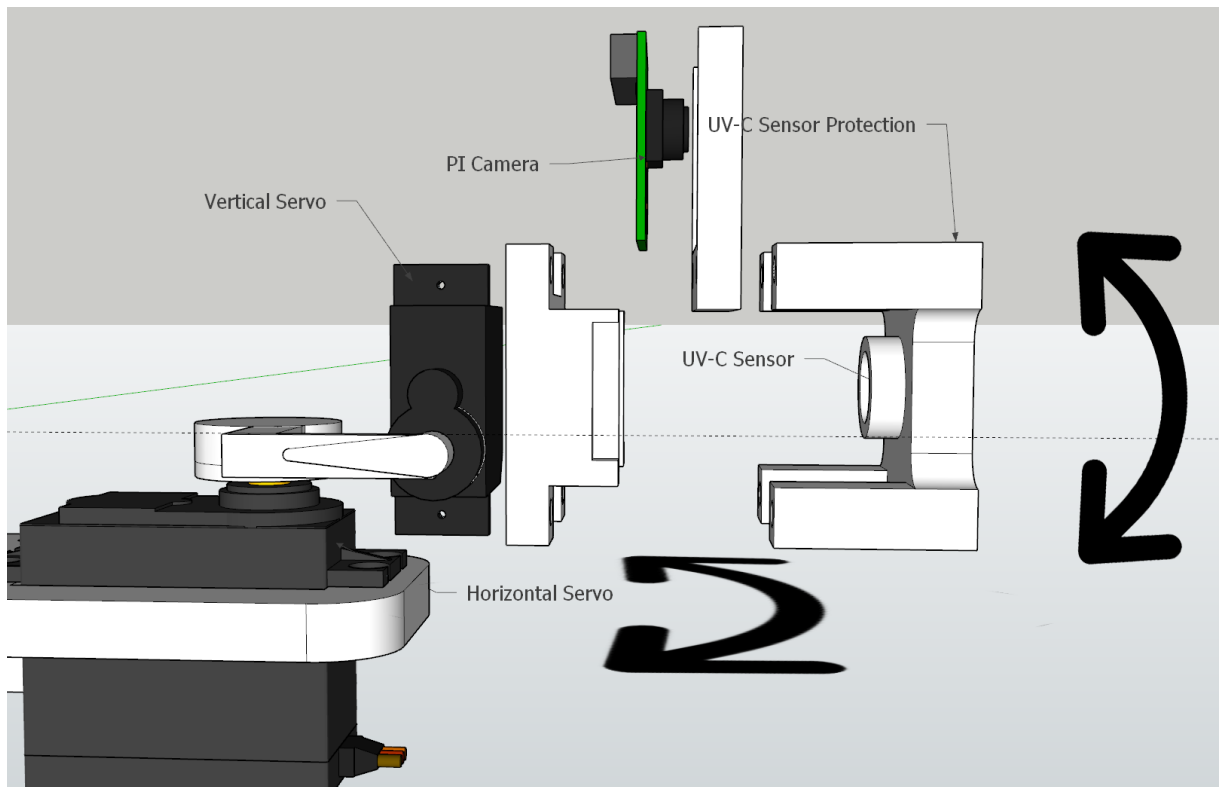
Figure 5-2. Head Movement

The servo motors of the head can be moved with a speed of up to 0.2s/60º, but our sensor has some limitations: it requires 0.069s for a single measurement. The entire matrix is comprised of 5600-point readings, leading to reading times of 387 seconds for the entire reading cycle.

After putting everything together, in Figure 5-3 is shown the system's head including the moving head, the two cameras, one static (ESP32-CAM) and one moving together with the UV-C sensor (Pi Camera).
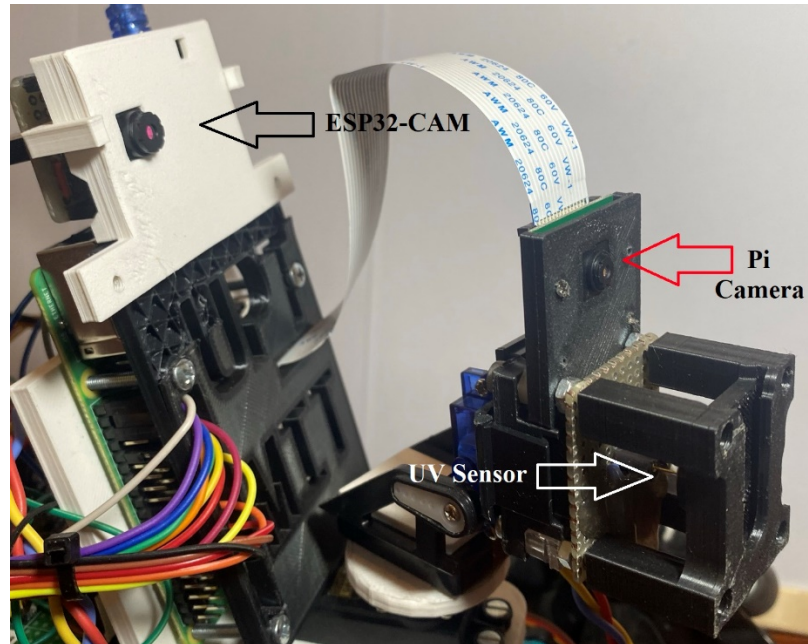
Figure 5-3. System's Moving Head

5.1.2. Cameras

The platform's head has two cameras attached to it but only one can be used at a time. The Raspberry Pi camera shown in Figure 5-4.a is connected directly to the Raspberry Pi through a ribbon cable and has a resolution of 3280x2464 pixels for still images and 1920x1080 pixels for video recording/streaming with 60 frames per second.

The OV2640 camera of the ESP32 shown in Figure 5-4.b is connected directly to the ESP32's circuit board and has a resolution of 1280x1024 and can be used as stand-alone.
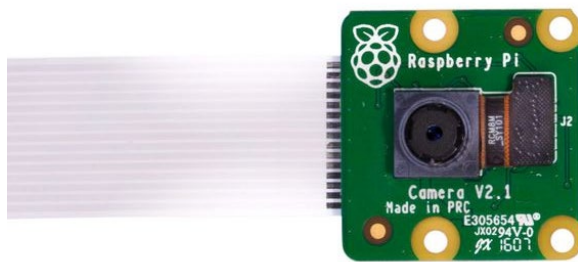
Figure 5-4. (a) Raspberry Pi Camera V2.1   (b) OV2640 Camera

The advantages of using an ESP32 over the Raspberry Pi and camera:
- Lower cost
- Stand-alone once programmed
- Lower power consumption
- Smaller foot-print
- Camera and controller share the same circuit board, it does not require any cables between camera and controller

Advantages of using the Raspberry Pi camera over the ESP32 one include:

- Higher photo and video resolution
- Can better process information, such as big matrices.
- Does not require internet connection, it can work without internet or through an offline router

18

- Higher transmission distance due to the bigger antenna and newer Wi-Fi chip
- Bluetooth availability
- Does not require a separate programmer
- Multiple control options

The ESP32 requires a programmer in order for it to function correctly. We are using a FT232RL FTDI programmer for uploading programs to the ESP32 shown in Figure 5-5. It is only required when uploading software to the ESP32, it is not required after.
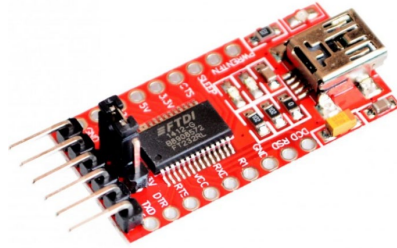
Figure 5-5. FTDI FT232RL USB UART IC

With the ESP32 being a stand-alone PCB, an adaptor to the main circuits is required.
In Figure 5-6 is represented said adaptor, comprised of a 6-wire cable for communications between the ESP32 and the rest of the circuit and a small PCB adaptor between the EST and the cable.
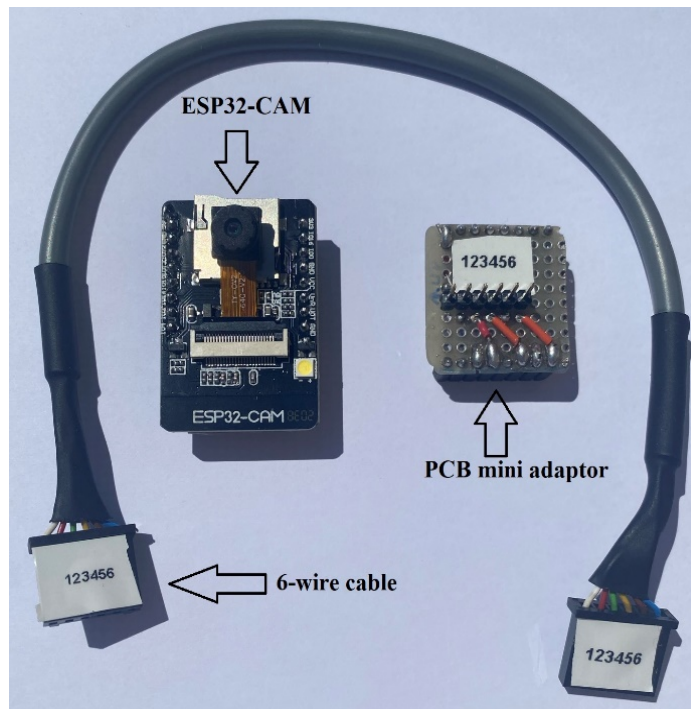
Figure 5-6. ESP32-CAM Cable and PCB Adaptor

The 6 wires connecting the ESP32 to the rest of the circuit are the following with the connections between the ESP, the FTDI and the Arduino Nano shown in Figure 5-7:

- +5V
- +3.3V
- GND
- RX – receiver line
- TX – transmitter line
- IO0 – for programming

For programming the ESP32, GPIO0 needs to be pulled-down (GND) before trying to upload the program to it. This is done by a jumper between the GPIO0 and GND.
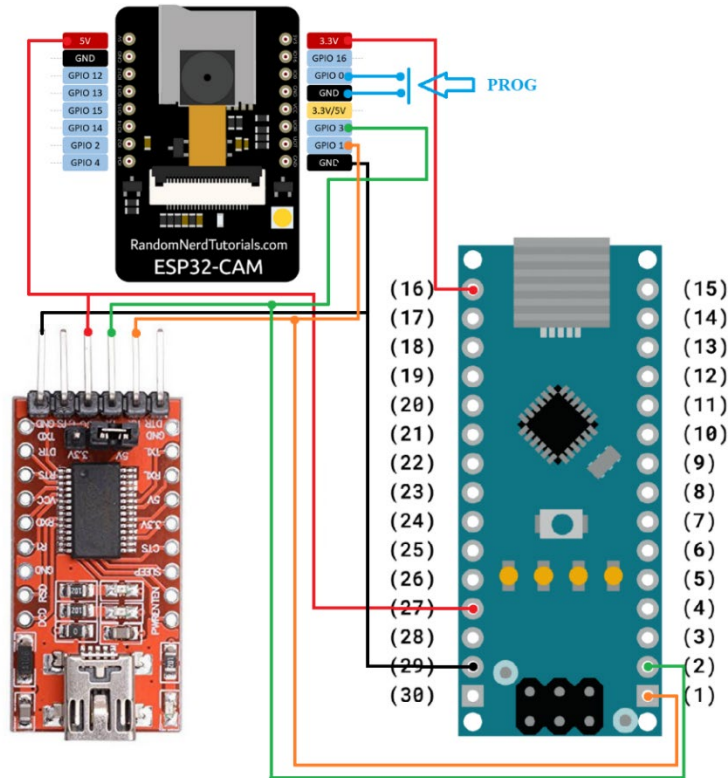
Figure 5-7. ESP32 to FTDI to Arduino Nano Connection Diagram

The ESP32 is able to read and keep in its memory all the data received from the Arduino. It has a memory of 32 Mbit that leaves enough room for the web server, the matrix data and other functions. It will still receive one row of the matrix at a time due to Arduino Nano memory limitations. After receiving every single row from the Arduino, a stop-bit is sent from the Arduino to the ESP in order to let it know the scanning has been completed.

In normal-mode operation, the ESP32-CAM is mounted at the back of the head and is static (i.e., it does not move when the head moves). This is done as a backup to the main camera in case of signal loss or frames-drop when transmitting through walls or high-interference mediums.

5.1.3. System Movement

In terms of moving, the platform has special wheels that do not require steering the front or back wheels like in a conventional RC car in order to steer left or right. The wheels shown in Figure 5-8 feature a double-cylinder structure made of hard rubber that is able to freely move around and is placed at a 45° with respect to the drive train. Those wheels are placed in a mirror configuration across the platform so that when two opposing wheels are driven in the same direction, the platform will move forward/backward as in a conventional RC car as opposed to sliding to left/right. Each wheel is powered by a dedicated DC motor for a total of 4 motors.

Figure 5-8. Platform's Wheels with Cylinders

This configuration allows for movement in all axes of direction, front/back, left/right, diagonally and rotate in place as illustrated in Figure 5-9, depending on the command sent to the drivers. Each wheel has its own electric motor and gear box.

Figure 5-9.a. Front   b. Sideways   c. Diagonally   d. Rotate in place
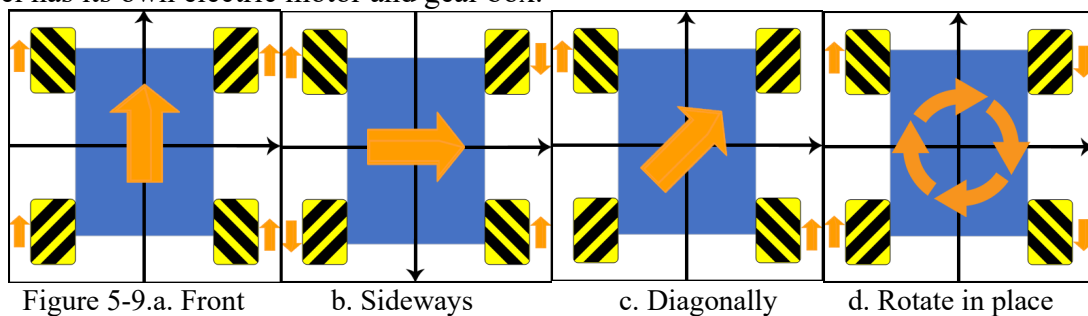
5.1.4. Power Supplies

For powering the entire system, we need two types of batteries. One for the electrical motors and one for power the rest of the circuit: the Raspberry Pi, the Arduino Nano, the ESP32, RC receiver.

For powering the motors, a single double-cell Lithium-Ion of 3.7V each is being used for a total voltage of 7.4V and a capacity of 1.3Ah as shown in Figure 5-10.

Figure 5-10. 7.4V Li-Ion Battery Pack

The battery pack of the motors is placed in a compartment located at the bottom of the car, under all the circuits.

For powering the rest of the system, a power-bank is attached to the back of the car using a 3D printed support as shown in Figure 5-11. The support screws onto the base support located in the middle of the platform. This power-bank is a 12Ah battery from Huawei capable of driving only the system for a maximum of 8 hours.
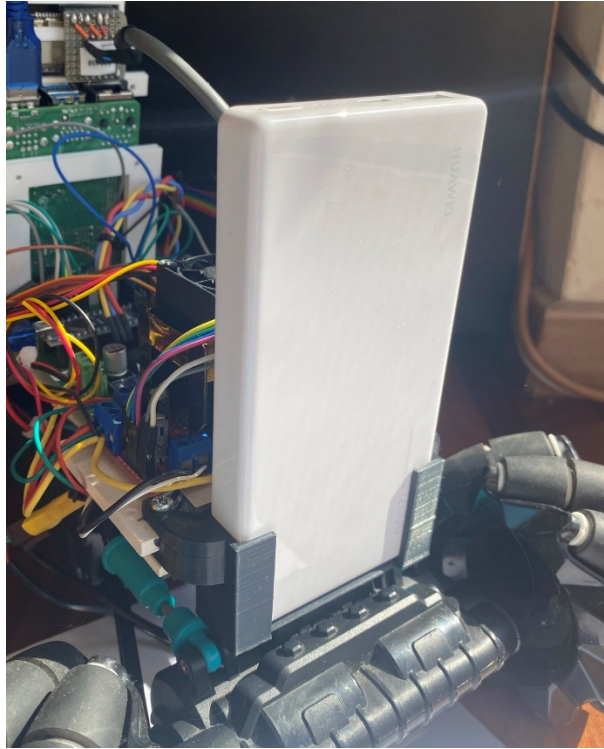
Figure 5-11. 12Ah Huawei Power-bank

This type of power-bank is directly connected to the Raspberry Pi 4 through a USB-C cable but can also be connected through a USB-A to USB-C cable (the Raspberry Pi 4 requires a USB-C connection).

If a smaller form-factor is required, either because of the main power-bank exceeds the desired weight or dimensions, a smaller power-bank can be used as shown in Figure 5-12. The smaller battery has a capacity of 2.6Ah and can power the entire system for less than an hour and is connected to the Raspberry Pi through an USB-A cable.

Figure 5-12. 2.6Ah Generic Battery and 3D-printed mount

This power-bank is to be mounted on the exact same spot as the bigger one and replaces it.

5.1.5.Controllers

In order to control the platform's system, remote controllers are needed. Two different remote controllers have been implemented: the PlayStation DualShock 4 controller through the use of Bluetooth and the MC6C remote controller through wireless.

The PS4 controller is more accurate, having a precision of 16 bits but has a lower transmission distance (8-10m) especially if there are walls or obstacles between the remote and the receiver.

The DualShock 4 controller connects directly to the Raspberry Pi's Bluetooth chip without any external hardware. The key-mapping for this is illustrated in Figure 5-13.
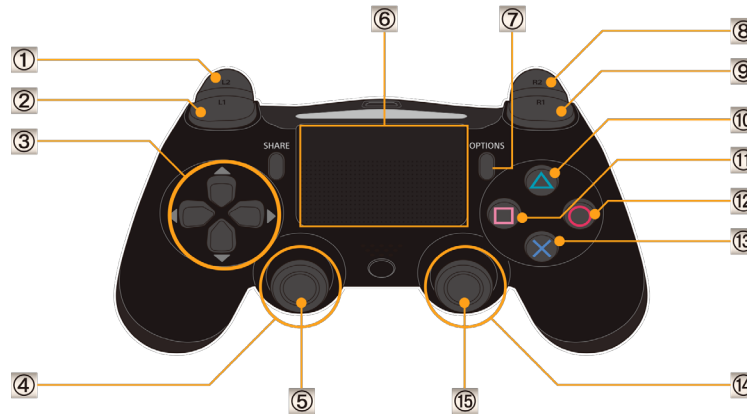
Figure 5-13. PS4 DualShock 4 Key Mapping

The left joystick (noted with "4") is responsible for controlling the left motors of the platform (both front and back) while the right stick (noted with "14") is responsible for controlling the right motors of the platform. The four buttons located in the left part of the controller and noted with "3" are the ones who control the head movement bi-directionally. Starting the measurement process is done by pressing the R2 trigger button (noted with "8" in the diagram).

The track pad (noted "6" can also be used as a mousepad for the Raspberry Pi if enabled.

The MC6C shown in Figure 5-14 has a lower precision of 10 bits but has a greater transmission distance of 500-1000m. With both remote controllers, the user can control the platform in all axes of direction, the sensor's head and control the UV-C measurements.

Figure 5-14. MC6C Remote Controller

The left joystick of the controller (elevator/rudder) controls the two motors on the left of the platform while the right stick (aileron/throttle) controls the two motors on the right of the platform. Both

joysticks have two axes of movement, up/down and left/right but we are only using the analog up/down part of it due to the platform not having steering wheels.

The joystick on the right of the controller also controls the moving head when the "switch 2" is not in the zero position. The switch 2 is responsible for switching between controlling the driving motors and controlling the servo motors of the head. When said switch is in the zero position, the driving motors are controlled; when it's in the up position, the servo motors are driven at a higher speed (5 steps in 200ms) for faster head transversal; when it is in the down position, the servo motors are driven at a lower speed (1 step in 200ms) in order to provide more fine tuning and accuracy.

Switch 3 is responsible for starting and stopping the scanning/measurement process cycle. When the "switch 3" is in the up position, the system will start measuring in the indicated mode (single mode or matrix).

We will be using the MC6C controller by default from here unless specified otherwise.

The MC6C needs a wireless receiver such as the MC6RE with the 6 channels info shown in Figure 5-15.

	CH	Airplane	Car
1	Ch1	Aileron	Right Motors, Left/Right
2	Ch2	Elevator	Left Motors, Up/Down
3	Ch3	Throttle	Right Motors, Up/Down
4	Ch4	Rudder	Left Motors, Left/Right
5	Ch5	Landing Gear	N/A
6	Ch6	Flap	Servo Toggle
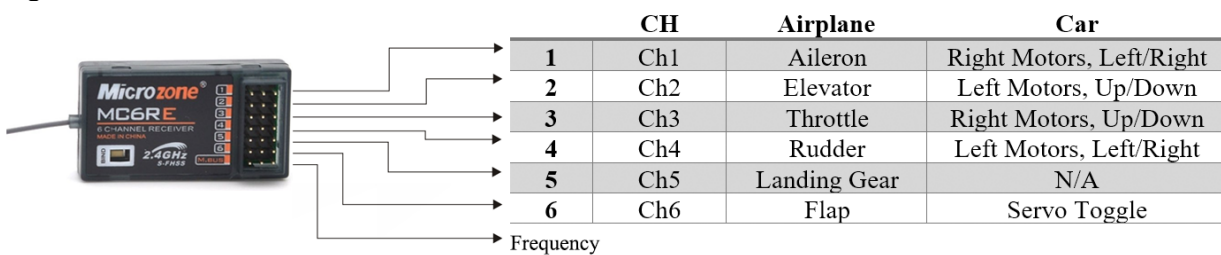
Figure 5-15. MC6RE 6-channel receiver

This receiver is equipped with 6 controllable channels, each having 3-pins headers, one for power (+5V), one for ground (GND) and one for each channel's signal. These pins will be connected directly to the Arduino Nano GPIOs as shown in Figure 5-16.
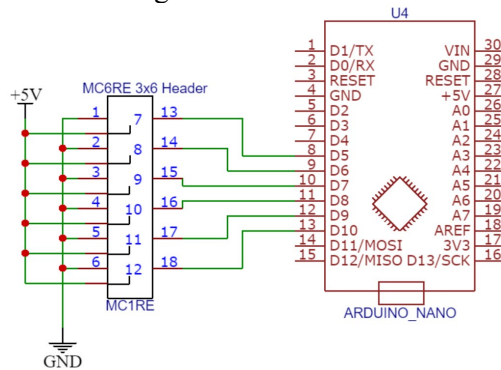
Figure 5-16. Arduino – MC6RE circuit connection

5.1.6. Drivers

In order for us to control such large power consumers as the motors that require approximately 2A each, the use of special motor drivers is required. In our case, we are using the L298N dual motor driver shown in Figure 5-17. A pair of this drivers is needed for controlling all motors; each driver is able to bi-directionally control 2 motors and satisfy the need of the motors.

24
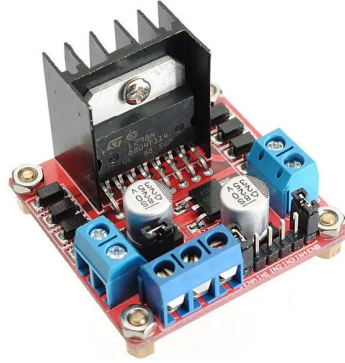
Figure 5-17. L298 Motor Driver IC with Heatsink

Those motors are mounted at the back of the car, far from the main controller of the platform. The motors drawing such a big amount of power from the batteries, from formula 5.1 we get a maximum of around 89 watts that will be outputted by the driver, where n is the number of motors used, in our case 4. If the motors are stuck almost all this power will be converted into heat. In order to prevent this heat from damaging the circuits, a bigger heatsink was installed on the driver and an additional fan was added on top for air circulation as shown in Figure 5-18.

$$P = V * I * n \qquad\qquad\qquad (5.1)$$
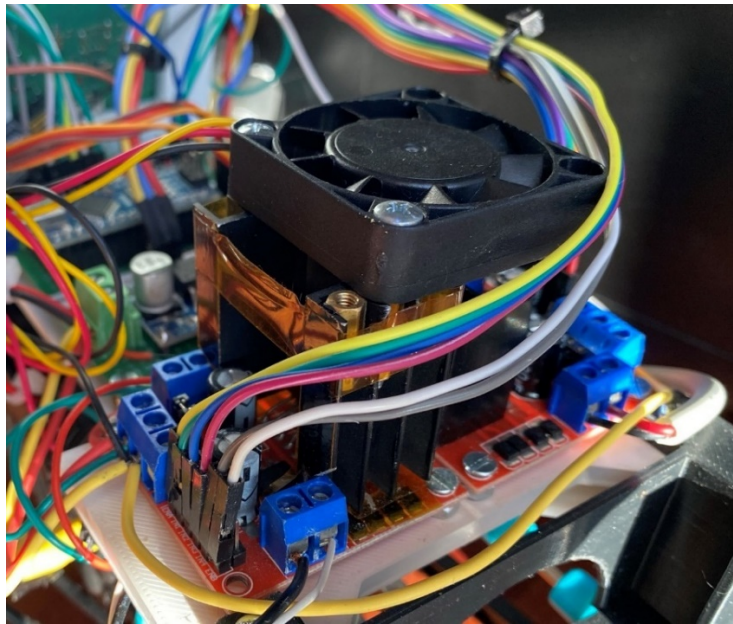
Figure 5-18. Motor Drivers and Heatsink with Fan

The fan can be turned on and off by a button present on the side of the platform.
A comparison between the old heatsink and the new heatsink can be seen in Figure 5-19. The new heatsink is approximately 3.7 times bigger than the old one.
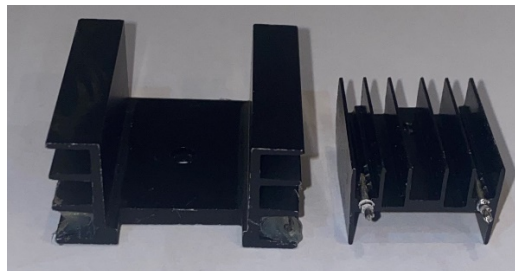
Figure 5-19. New Heatsink (left) and old heatsink (right).

These drivers are the backbone for proper functioning of the motors. The motors will not be able to be controlled without them, doing so will result in burning the Raspberry Pi. The circuit diagram of both motor drivers is presented in Figure 5-20
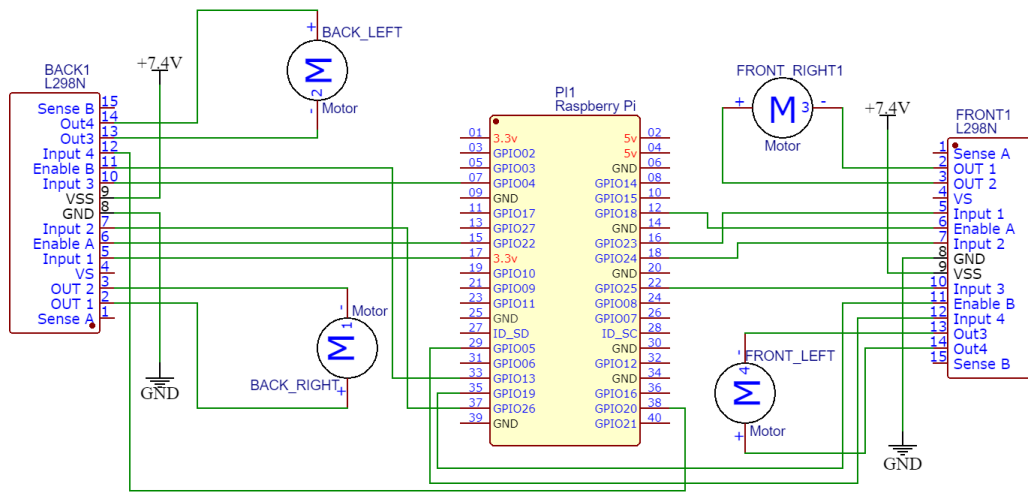
Figure 5-20. Motor Connection Circuit

5.2. Software Implementation

The system takes advantage of a multitude of software programs and libraries. The system can also be controlled through software only if the remote controllers are not available.

5.2.1. Raspberry Pi

The Raspberry Pi 4 is where the hardware and software are centralized. The main part of the software is the python server responsible for communication between all devices. The main python server includes a smaller python camera web server trough the "*PiCamera*" library accessible from anywhere. The camera server takes care of capturing the video feed from the hardware Pi camera and redirecting it to an actual web server through a streaming server included in the *PiCamera* library.

Camera parameters can be directly modified from the camera server, making use of the function shown in Figure 5-21. The parameters that can be modified include, but are not limited to: server address (if different than the local address), server port, camera resolution, framerate, orientation, rotation, format (format should be left on "mjpeg" for streaming videos, otherwise problems such as time delay and compression artifacts can arise), filters, etc.

```python
with picamera.PiCamera(resolution='1280x720', framerate=24) as camera:
    output = StreamingOutput()
    camera.rotation = 180
    camera.start_recording(output, format='mjpeg')
    try:
        address = ('', 8000)
        server = StreamingServer(address, StreamingHandler)
        server.serve_forever()
    finally:
        camera.stop_recording()
```

Figure 5-21. Camera Configuration Object

The python server requires certain configurations in order to function properly such as:

- The Arduino Nano needs to be connected to the Raspberry Pi through a USB cable or through serial pins

- File location for the text file containing sensor measurement data (folder on Desktop by default)

- File location for the image taken from the camera (folder on Desktop by default)

- 2D matrix dimensions (default value of 100x56)

- The serial port of the connected Arduino Nano

- Serial transmission speed

The last two parameters can be configured by modifying the line shown in Figure 5-22 and the server will not work at all without configuring those parameters correctly. The rest of the parameters come with a default value and should work in most cases.

```
ser = serial.Serial("/dev/ttyUSB0", 115200, timeout=0)
```

Figure 5-22. Python Serial Configuration

If the PS4 DualShock controller is to be used instead of the MC6C controller, an extra library called "*pygame*" is needed and a special driver called "*DS4Drv*". The *DS4Drv* needs to be started before starting the python server and needs to be running for the entire lifetime of said server. Failure to do so will result in disconnecting the DualShock controller and halting the program. If this is to happen while either joystick on the controller is not in a stall position, the motor drivers will remain enabled at that value and keep running.

The purpose of the DS4Drv driver is to translate Bluetooth information received by the Wi-Fi chip on the Raspberry Pi from the DualShock controller into commands that are interpretable by the python server. Python doesn't support said commands by default and so the use of the *pygame* library is needed. This library is able to emulate our server like a video game that is controlled by a PS4 controller. A major drawback of this library is the need of a physical display attached to the Raspberry Pi in order for it to function. The library will prevent the server for starting up because of this when running from a remote connection. This problem can be overcome with the use of a web control panel that emulates the remote display as one attached directly to the Raspberry Pi but it is not a perfect solution so we decided to replace the DualShock controller with the MC6C controller. In Figure 5-23 is illustrated the execution flow of the python server located on the Raspberry Pi that is responsible for interconnecting the Arduino Nano, the motors and the web cameras.
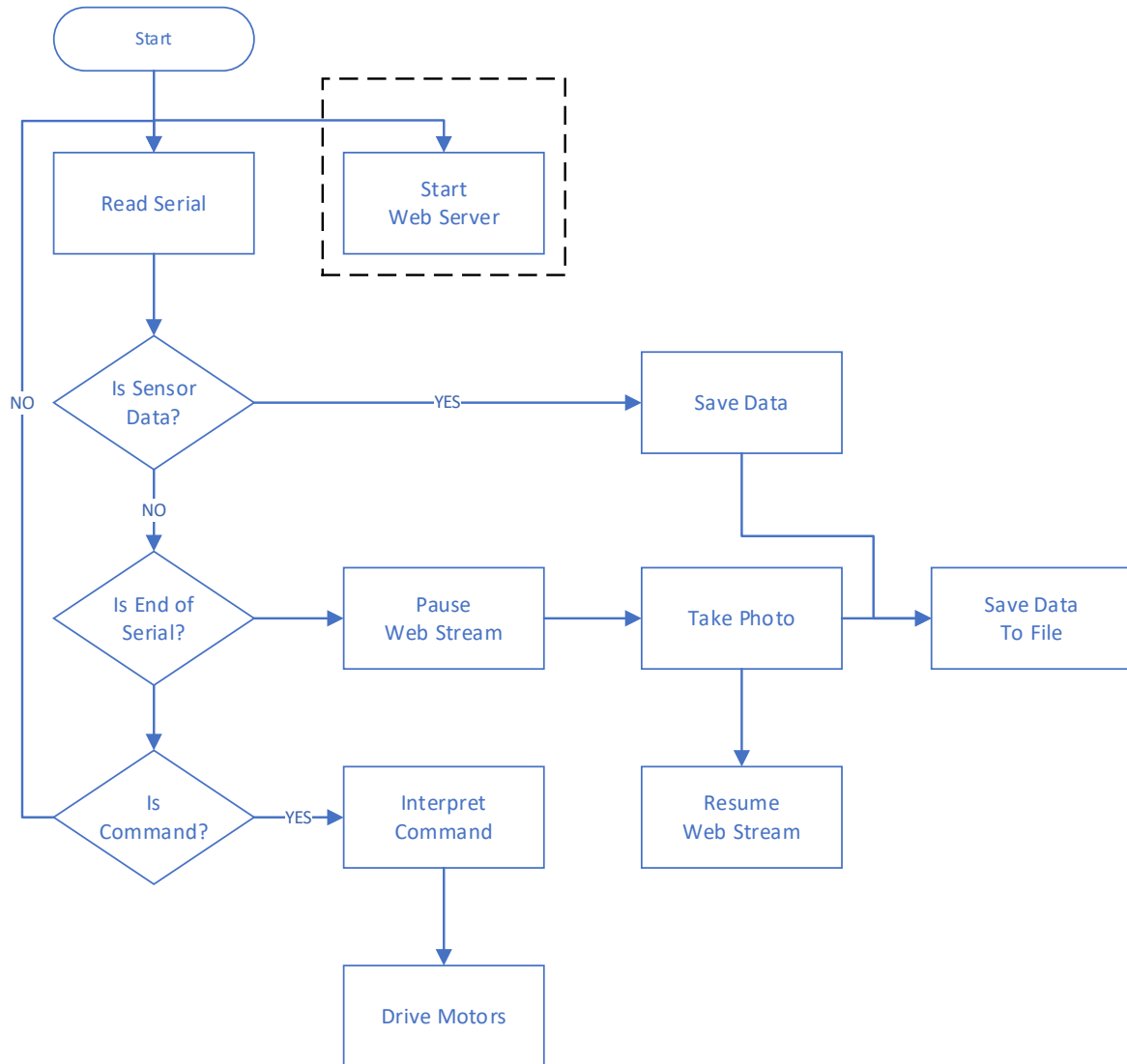
Figure 5-23. Python Execution Flow – Serial Communication

The execution flow is valid for when using the MC6C controller and commands are received serially from the Arduino Nano.

If the head camera is active when controlling the system, the web streaming service must be paused/stopped when taking an image. This is because the Raspberry Pi and Pi camera does not support multiple connection streams such as the web stream. This is done automatically when a scanning routine has finished by the python server. The user present on the web page with the camera stream on will notice the video stream blocking for a short period of time (approximately 1-2 seconds) when the routine finishes and then it starts again.

The Raspberry Pi is only capable of reading digital signals and the sensor we are using is an analog one. Because of this, some sort of analog-to-digital (ADC) converter is needed, in our case an Arduino Nano.

5.2.2.Arduino Nano

In Figure 5-23 is illustrated the Arduino Nano program execution flow. When the Arduino is powered on, it will begin to move the servo motors to a preset position, in the middle at an angle of 90° to the platform. After the servo motors have been initialized, the Arduino will start listening for commands either from the Raspberry Pi or from the MC6C controller. The Raspberry Pi will send command via serial communication from the Bluetooth DualShock 4 controller, while the commands from the MC6C controller are taken directly from the MC5RE receiver. This means that the platform can be controlled by both remotes (DualShock 4 and MC6C), they are not mutually exclusive. The commands that are received from the MC6C controller will be interpreted and, if the commands dictate the driving motors should be moved, said command is sent to the Raspberry Pi. If the command is a servo command, it will not be sent to the Raspberry Pi but will act directly on the servo motors attached to the Arduino Nano. If the command received, either through the DualShock 4 controller or through the Raspberry Pi or through web via the Raspberry Pi is a START_SCAN command, the Arduino will start scanning for UV-C light.
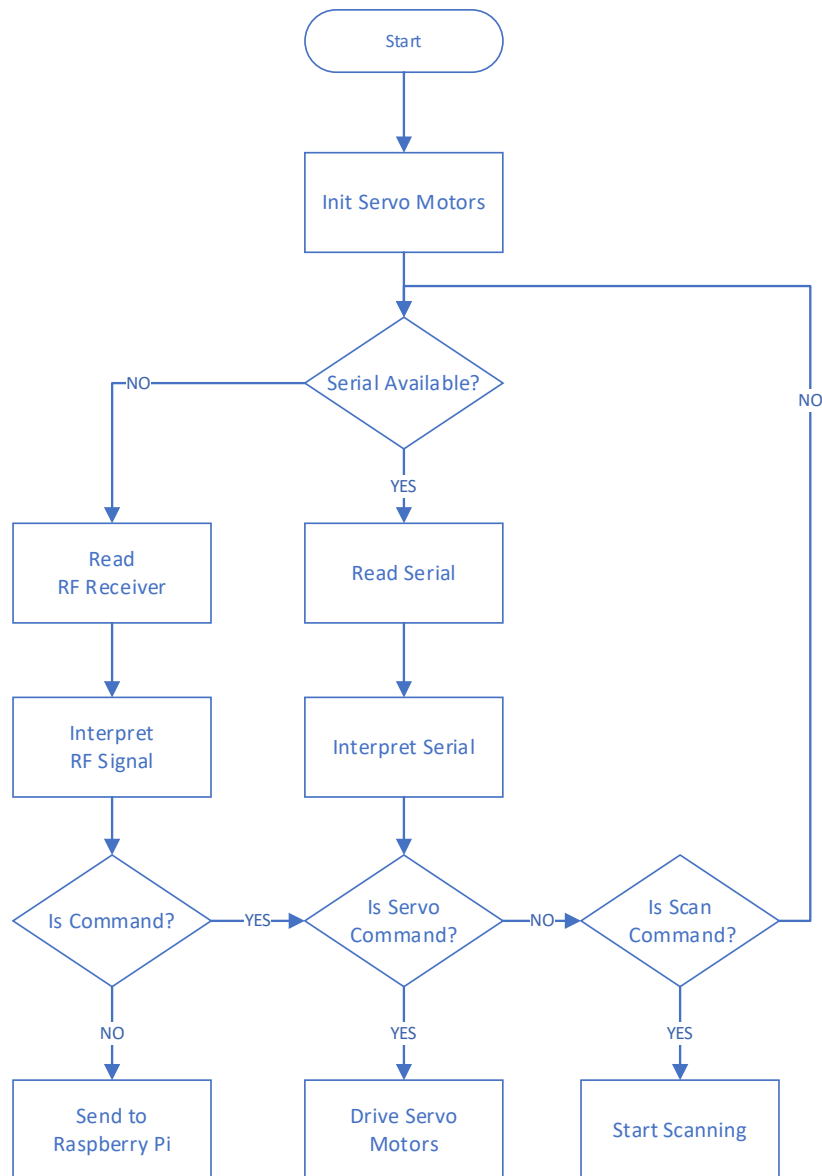

Figure 5-24. Arduino Program Execution Flow

29

The Arduino Nano is capable of reading analog signals with a resolution of 10 bits and values between 0 and 1023 with a total number of 2^{10} possible values. The basic difference between an analog signal and a digital signal is shown in Figure 5-25.
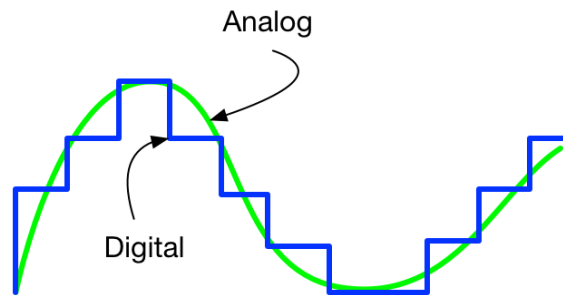

Figure 5-25. Analog vs. Digital

With a resolution of 10 bits, we get an accuracy of 0.048V at a supply voltage of 5V and 0.032V at a voltage of 3.3V or ±0.96%.

The Arduino Nano is responsible for reading analog data from the UV-TIAMO-C6 sensor mounted on the head. The program running on the Arduino will wait for a start signal via serial communication from the main board (Raspberry Pi or ESP32) or by reading the state of an input connected to a relay if using the default controller of the RC car before starting measurements. Once the signal has been received, the measurement cycle will start. Once the cycle has been started for a 2D matrix measurement, the servo motors will start moving to the initial measurement position which is in the left-most, upper corner of the matrix (position 1). This path is illustrated in Figure 5-26.

1	2	3	4	5	6	7	8	….	100
200	199	198	197	196	195	194	193	…	101
201	202	203	204	205	206	207	208	…	300
400	399	398	397	396	395	394	393	…	301
…	…	…	…	…	…	…	…	…	…
5501	5502	5503	5504	5505	5506	5507	5508	…	5600

Figure 5-26. 2D Matrix Traversal Path

Measurement starts at a predefined location on the double circular path and traverses the entire area line by line until the last point located on the opposite side of the imaginary grid. Each value that is received by the Arduino from the sensor is added into a vector and, once a line is finished, the entire vector is sent through serial communication to the Raspberry Pi or the ESP32. The Arduino will not fit the entire array that requires approximately 11.2Kb of memory while the Arduino has 32Kb of memory of which 2Kb are required by the bootloader, 2Kb are dynamically reserved for global variables in the Arduino program and 19Kb are used by the Arduino program itself. Adding all up we are left with 9Kb of free space in the Arduino Nano and will not fit the entire array.

The UV-TIAMO-C6 sensor will not measure ultraviolet radiation instantly, instead it requires a wait time of 0.069 seconds for each measurement reading. We have a total of 100 points horizontally and 56 points vertically for a total of 5600 points to measure for a 2D matrix reading in a total of 386.4 seconds. We are giving the sensor a margin of error of 0.001 seconds (1.44%) per reading leading to a measurement time for a single value of 0.07 seconds. Taking this into consideration, we are able to do a complete scan in 392 seconds or just a bit over 6 and half minutes.

The Arduino Nano is also responsible for controlling the two servo motors that move the platform's head.

5.2.3.Processing

Processing is an open-source platform, library and integrated development environment (IDE) for creating software and visual design. We are using it to create the 2D matrix drawing from raw values from the server.

The Processing software has two modes of operation: one for the ESP32 where it will wait and listen for serial messages sent from the Arduino through the ESP32 to the serial output. It will receive raw sensor values one line at a time and construct a 2-dimensional array. Part of an example of how those values will look like is shown in Figure 5-27. Before starting to gather sensor values, array size must be received by the Processing, otherwise the default values of 100 and 56 will be used for allocating memory for the array. The array is dynamically created with each line that is received. The program will finish when a stop command is received. After the program finishes receiving all the data, the drawing part of the software starts.

```
110 104 71 37 16 15 16 20 26 27 28 29 32 35 37 39 41 42 45 47
10 12 13 14 17 19 21 24 26 28 29 31 34 34 37 38 40 42 43 46 4
8 8 6 7 8 11 13 16 17 19 19 23 24 29 29 32 33 34 36 39 42 42
11 13 15 17 19 20 24 26 28 30 32 33 36 38 40 42 44 45 47 50 5
9 8 8 6 7 10 14 16 18 19 22 23 26 29 30 33 35 37 38 42 42 44
13 14 15 18 20 22 24 27 30 31 33 35 37 39 41 43 45 47 51 54 5
10 10 9 9 8 11 16 18 19 21 22 25 28 30 32 35 37 36 40 42 43 4
12 14 16 19 20 24 25 27 31 31 32 34 38 40 42 44 46 48 50 52 5
11 9 8 9 9 12 15 17 21 21 24 26 28 30 32 35 38 39 41 42 44 47
13 14 17 19 22 24 27 30 33 33 35 37 37 43 43 47 48 50 52 55 5
10 11 10 10 10 11 16 19 20 22 24 27 30 32 34 36 38 41 43 45 4
14 17 17 20 22 25 28 31 33 35 35 37 40 43 44 46 48 50 53 56 5
11 11 11 10 11 13 16 21 22 24 25 28 30 33 36 38 40 41 44 47 4
```

Figure 5-27. Raw Sensor Data Example

The drawing process will create a grid with the same dimensions as the array size (100x56 by default) with each cell having a black and white value depending on the sensor value. These color values range from 0 (white) to 255 (black) while the sensor values range from 0-1023. In order for us to have transposable data between the sensor value and the RGB value, a gain function has been implemented. The gain can be left on auto or set to manual, but setting it to manual is preferred when testing the same location because the gain function will keep the same gain coefficient across multiple testing points and provide more reliable data. A comparison between a low gain coefficient and a high gain coefficient is shown in Figure 5-28.
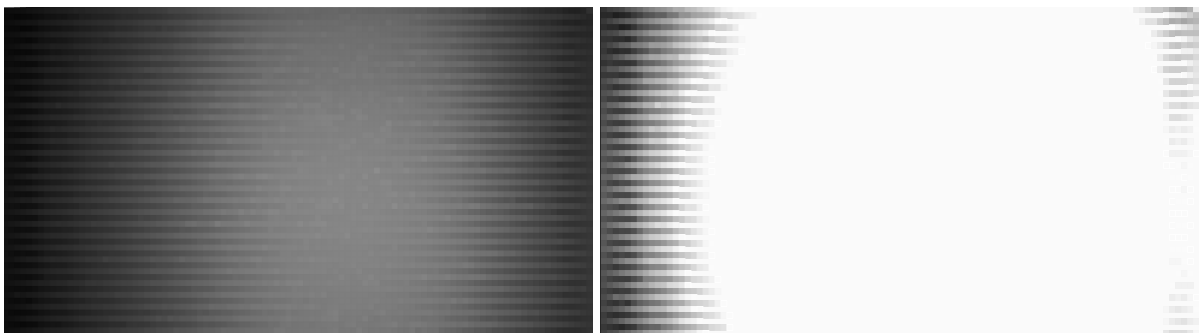
Figure 5-28.a Low Gain   b. High Gain

These results are based on the same set of values from the sensor, the only thing that is changed is the coefficient gain.

Using the Processing software in compatibility mode with the ESP32 will not provide image comparison between the generated greed and an actual photo from the camera.

Another way of using the Processing software is with the Raspberry Pi. As the Raspberry Pi will output a text file containing all sensor data and an additional photo taken at the end of the measurement process, a comparison can be made between the two. The software needs the two files, the text file and the image file generated by the Raspberry Pi, in order to function in this mode as opposed to listening to the serial port for incoming data and constructing the array on the go. In this mode, the

average of values greater than zero and the maximum values from those values is computed and displayed, and is shown in Figure 5-29. The upper part of the image contains the grid values generated by the software while the bottom part is an image taken at the end of the program's execution. Average and maximum values of the data is shown in the upper left-most corner.

average: 84

maximum: 140

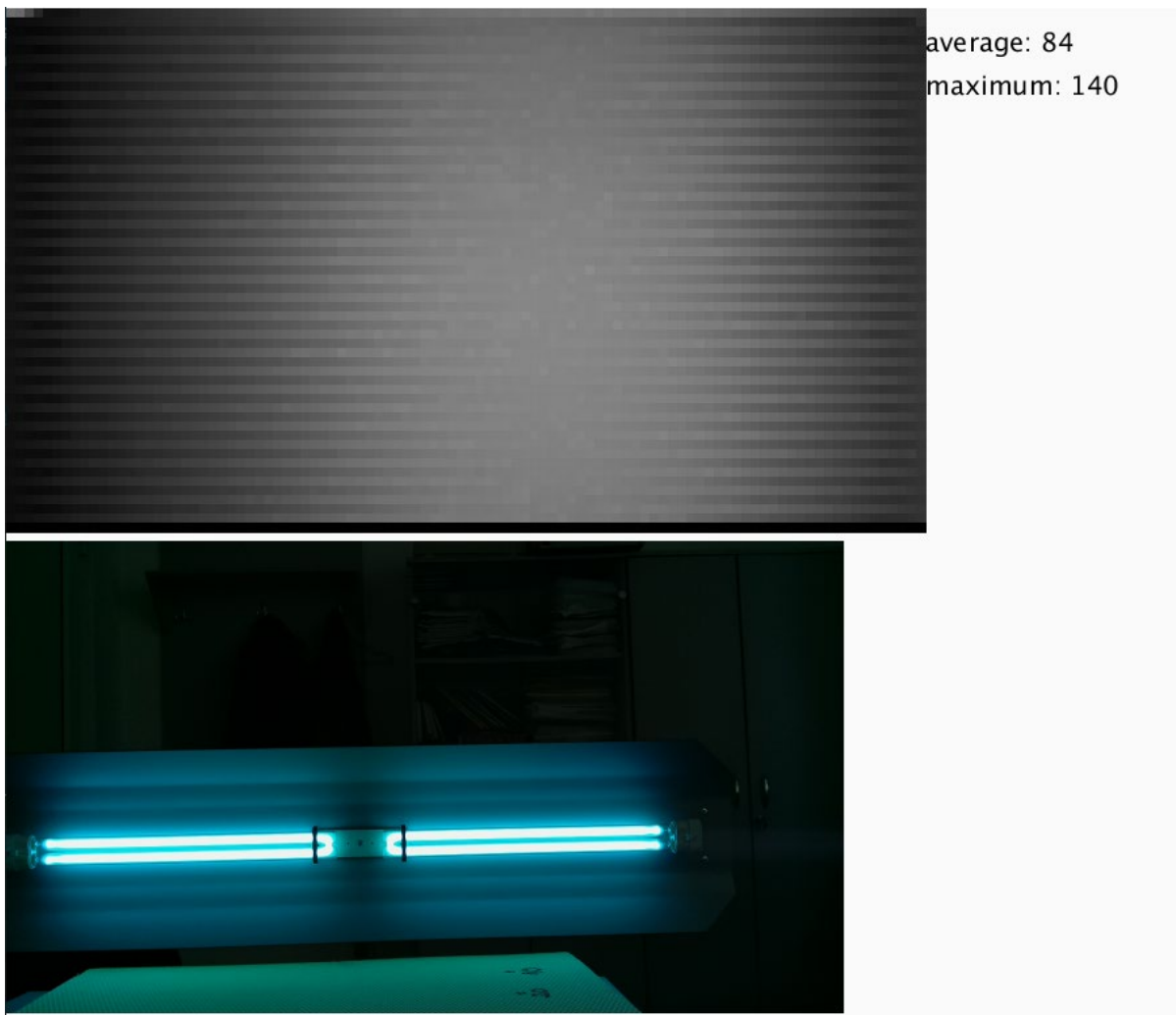Figure 5-29. Processing Example Output with Comparison

Using the Processing software manually is pretty straight forward. The user runs the program and is immediately prompted with two file dialog windows. The first dialog window will ask the user for an image file (the image captured by the Pi Camera when finishing a scan) and a text file containing the sensor data from the Raspberry Pi.

6. Test Results and Data

Several testing scenarios have been done in order to test the UV-C sensor's responsivity to ultraviolet radiation and are to be explained below.

It is important to not stay in the same location with the UV-C light source when it is powered ON. Short wave ultraviolet light is harmful to humans, direct exposure to the radiated UV light can lead to skin cancer, inflammation of the cornea of the eye and permanent vision impairment [21]. All safety precautions have been made during the testing process: humans were not present in the same room as the UV-C lamp and the room was well ventilated.

The first testing scenario includes a single, 25W mercury-based lamp. Several tests have been conducted from various distances

In the image shown in Figure 6-1, the testing environment containing the ultraviolet emitting lamp is shown. The UV-C light with a wavelength of exactly 253.7nm can be seen in the middle, upper part of the image. The image was taken at a distance of 2 meters from the light source.
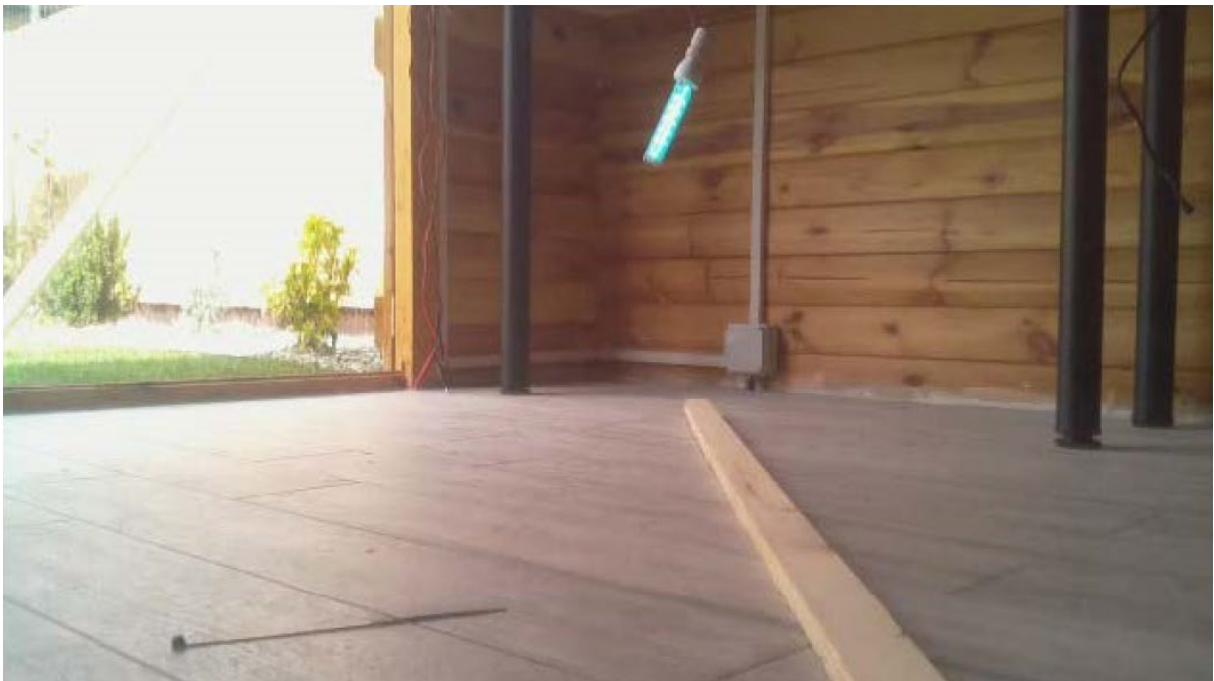
Figure 6-1. Testing Environment, One 25W Lamp, 2 m

In Figure 7-2 the various test results from different distances to the UV light source are shown. The tests were done in increments of 0.5m starting from 0.5m to the sensor and up to 2.5m to the sensor for a total of 5 tests.

The lamp used in this test is a generic UV-C disinfection lamp on which we don't know the exact radiation flux but is to be calculated later with sensor data.

This type of UV-C lamp has an E27 socket and is powered straight from the 220V wall plug.

Figure 6-2.a Grid Results from 0.5m
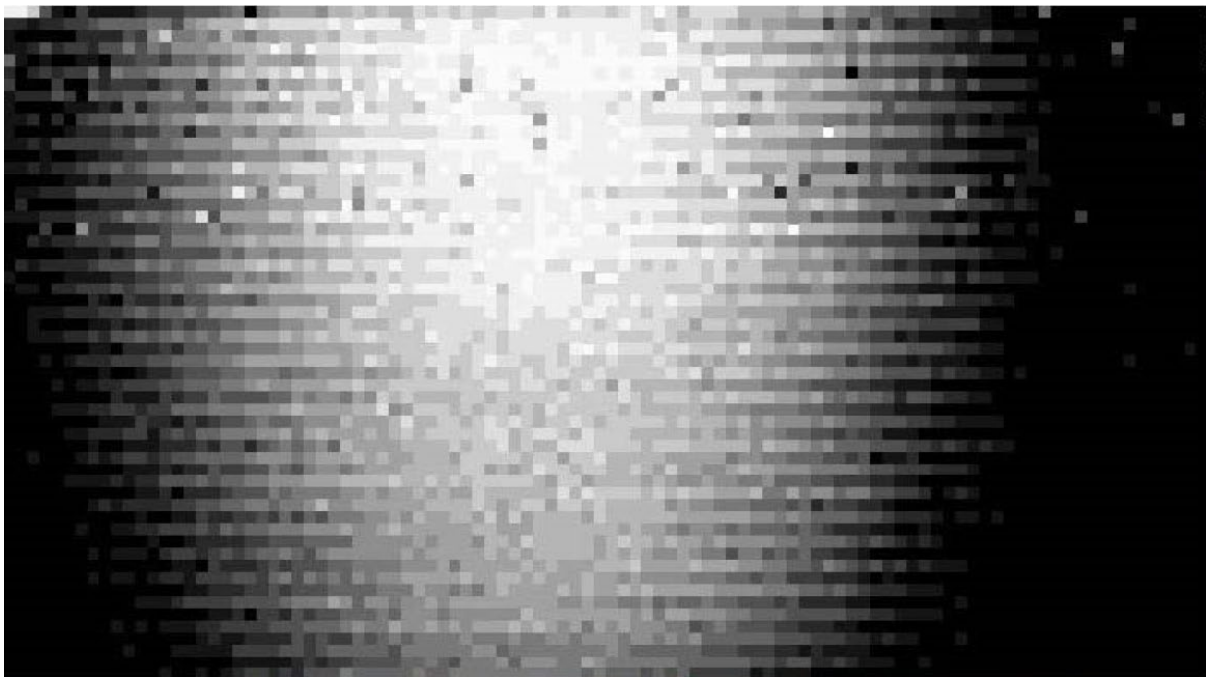
Figure 6-2.b Grid Results from 1m
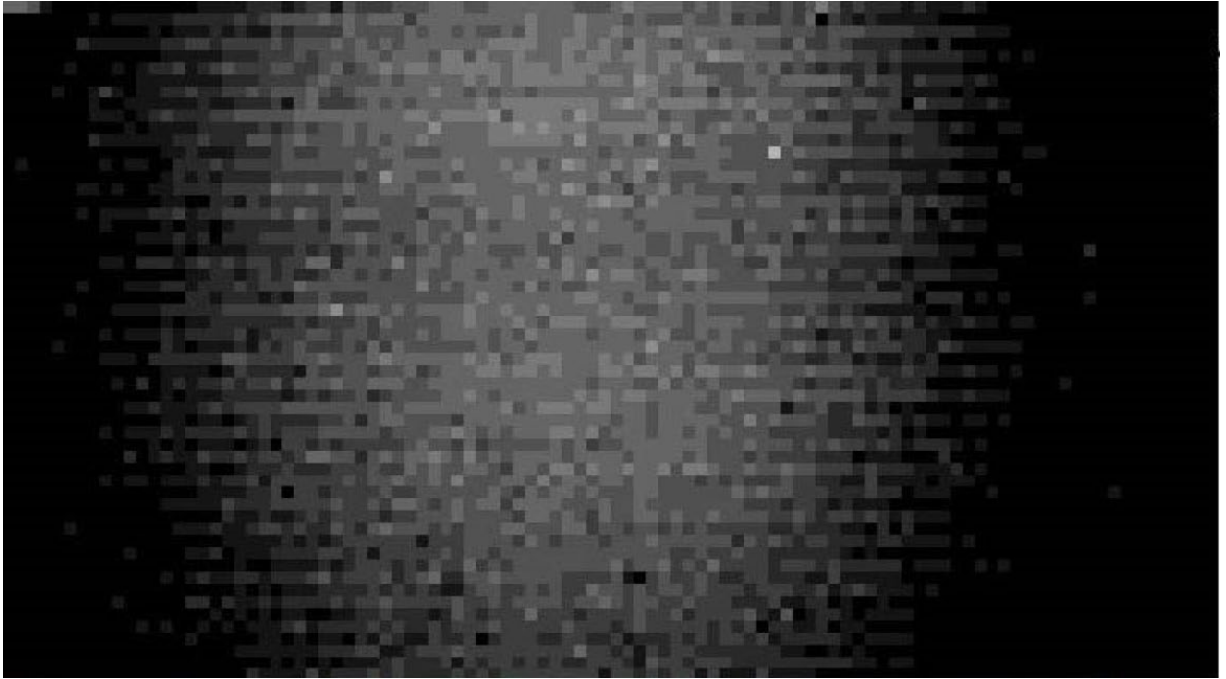
Figure 6-2.c Grid Results 1.5m
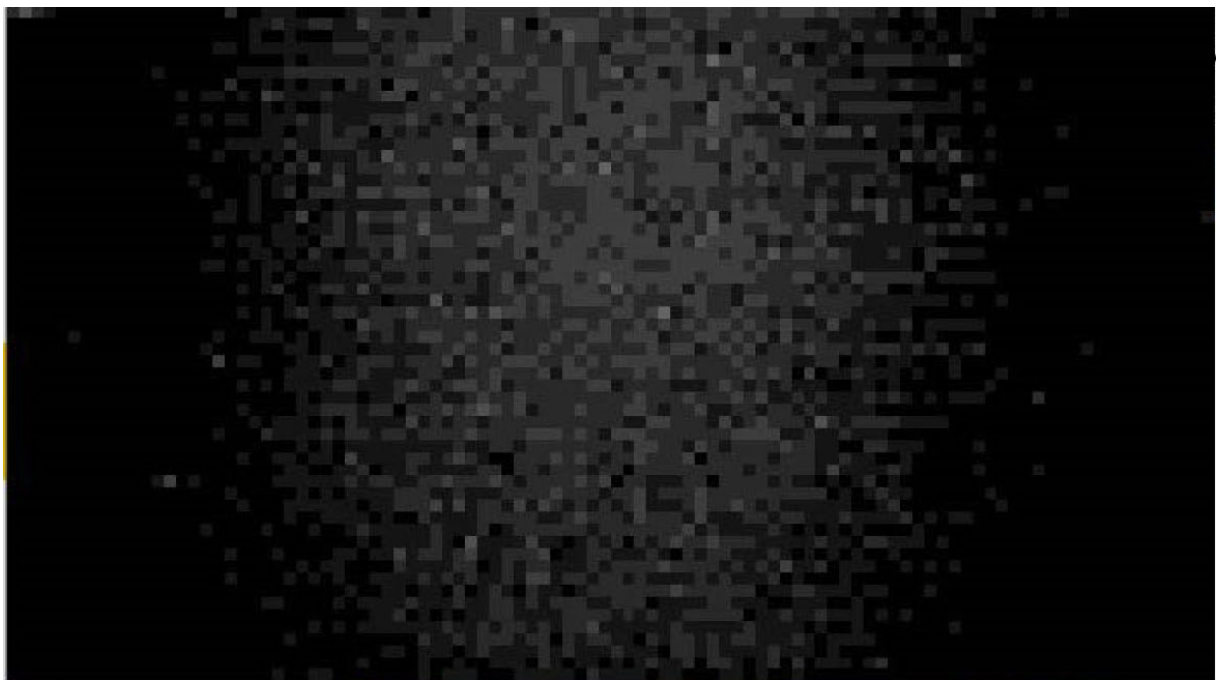
Figure 6-2.d Grid Results 2m
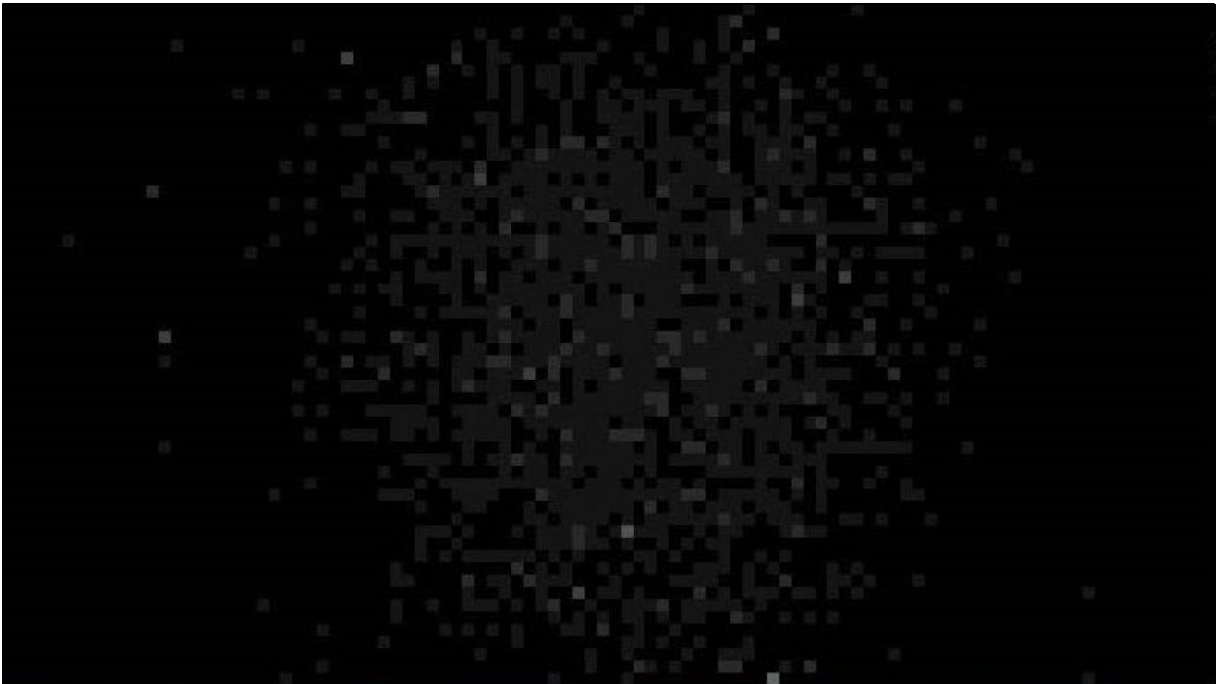
Figure 6-2.e Grid Results 2.5m

A conglomerate of UV-C light can be seen in the upper part of the image, exactly where the UV lamp is located. This conglomerate is reduced in size at an inversely proportional ratio with respect to the distance between the sensor and the UV lamp. The further away the sensor is from the lamp, the lower the intensity of the UV radiation.

In Table 6-1 tests results are shown from the various distances tested. With the tests being conducted at a voltage of 3.3V, we get a value of 0.0032V/division.

Distance	Average	Maximum	Average [V]	Maximum [V]
0.5m	17	44	0.0544	0.1408
1m	7	18	0.0224	0.0576
1.5m	3	9	0.0096	0.0288
2m	1	5	0.0032	0.0160
2.5m	1	5	0.0032	0.0160

Table 6-1. Single 25W Lamp Results

From these results we can compute the radiation coefficient loss based on distance shown in Table 6-2

Distance	Average [x]	Maximum [x]
0.5m-1m	2.42	2.44
1m-1.5m	2.33	2
1.5m-2m	3	1.8
2m-2.5m	1	1

Table 6-2. Distance Radiation Coefficient

We take this test data and put them in a chart shown in Figure 6-3 in order to have a better visual representation of said data.
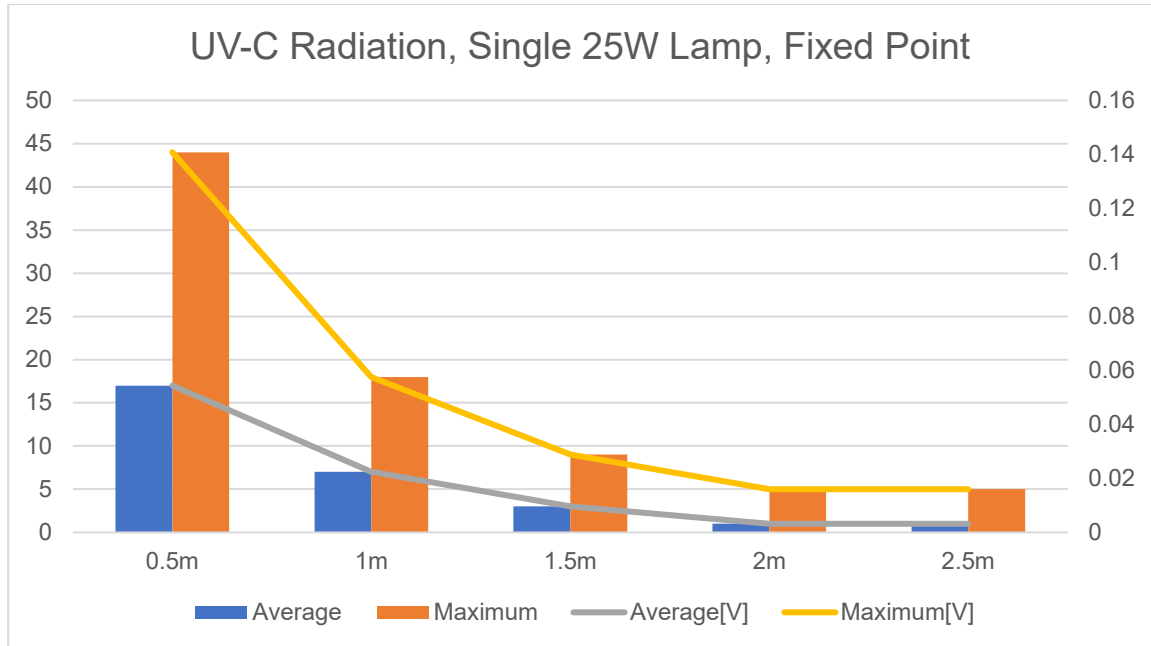
Figure 6-3. Single 25W Lamp Results Chart

As a baseline for our tests and in order to make sure everything works correctly, multiple tests were conducted from a distance of 1 meter with one and two UV-C lamps.

The 2nd testing scenario includes a single-lamp configuration with one 36W mercury-based lamp from a fixed point (i.e. the head of the platform does not move). In Figure 6-4 a single, 36W ultraviolet lamp with a wavelength of 253.7nm that is used during testing is shown. The tests were done with a reference voltage of 5V, from a fixed position.
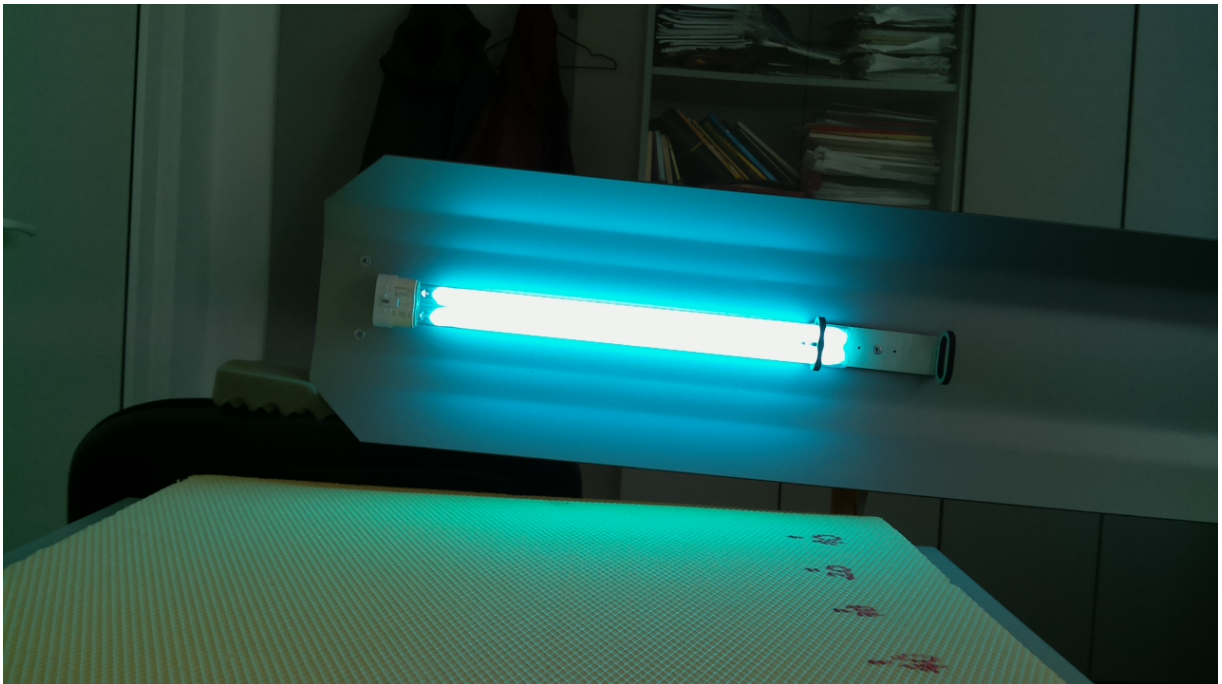
Figure 6-4. Testing Environment, One 36W Lamp, 1m distance

Next, we need to find the irradiance of the lamps used in testing. Irradiance is the amount of light that is hitting an object each second. Light irradiance is measured in $\mu W/cm^2$ or W/m^2. For the first testing scenario, we used a generic lamp without knowing the radiation flux of the UV lamp and thus being unable to calculate the irradiance on the sensor.

The lamp is powered by a HF-Selectalume electronic ballast as shown in Figure 6-5. This ballast is capable of powering a single PL-L lamp of up to 36W as the one we use.

Figure 6-5. HF-Selectalume 118/136 TL-D Electronic Ballast

Before starting to measure the irradiance on the sensor, we need to compute the distances between the sensor and the light source as shown in Figure 6-6 where P is the UV detector's location, B is the light source width and is a constant, A is half the width of the light source and is also constant and equal to 192.5mm, C is the distance between the sensor and the light sources and changes with every test with increments of 0.5m starting from 0.5m, α is the half the angle of the sensor with respect to the incoming light used in the irradiance formula mentioned earlier and is computed with each test.
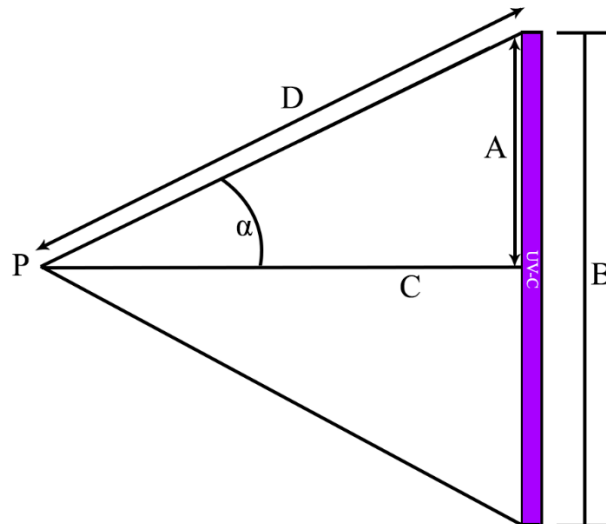
Figure 6-6. Test Setup Trigonometry

The formula for calculating the light irradiance is shown in (6-1) taken from [22].

$$E = \frac{\varphi}{2*\pi^2*B*C}(2\alpha + sin2\alpha) \qquad (6\text{-}1)$$

φ is the total radiation flux in Watts, A, B and C are known distanced between the sensor and the light source and the UV lamp diameter, D is computed using the (6-2) trigonometry formula while α is calculated using the (6-3) formula.

$$D = \sqrt{A^2 + C^2} \qquad (6\text{-}2)$$

$$\alpha = sin^{-1}\left(\frac{A}{D}\right) \qquad (6\text{-}3)$$

Below are the results for a single, 36W UV-C of 253.7nm light emitting lamp, from various distances with a total radiance flux of 110μW/cm^2. The tests were conducted from a distance of 0.5 meters, 1 meter, 1.5 meters and 2 meters. This set of tests was conducted with a reference voltage of 5V. For the various test distances, the respective values and distances are shown in Table 6-3 and are to be used later in the (6-1) formula.

C	D	α
0.5m (500mm)	0.535m (535mm)	0.367 (21.04°)
1m (1000mm)	1.018m (1018mm)	0.19 (10.89°)
1.5m (1500mm)	1.512m (1512mm)	0.127 (7.296°)
2m (2000mm)	2.009m (2009mm)	0.095 (5.451°)

Table 6-3. Distances and Angles

Testing on this single 36W UV lamp has been done from distances of 0.5m, 1m, 1.5m and 2 meters with the scan results and calculated irradiance shown in Table 6-4. Using this we can calculate the point at which the UV-TIAMO-C6 detector achieves the max irradiance of 1.8mW/cm² or 1800μW/cm². The single 36W lamp will irradiate the UV detector with a value of 1823μW/cm² from a distance of 0.2 meters from the sensor which is already over the max irradiance the UV detector can accurately interpret. Thus, the tests must be done from a distance greater than 20cm from the UV lamp.

We know from the UV detector's datasheet that the maximum irradiance the sensor can read is 1.8mW/cm² at a wavelength of 254nm and is achieved at 95% of the supply power which should not exceed 5V. The average irradiance in the table is the calculated irradiance assuming a linear progression at 1.8mW/cm² using the (6-4) formula where D_v is the value in volts taken from the UV sensor at various distances and is present in Table 6-4 while the expected irradiance is calculated using the (6-1) formula.

$$x_v = \frac{1800\mu W/cm^2 * D_v}{5} \qquad\qquad (6\text{-}4)$$

Distance	Average [RAW]	Maximum [RAW]	Average [V]	Maximum [V]	Avg. Irradiance [μW/cm²]	Expected Irradiance [μW/cm²]
0.5m (1_2)	253	307	1.235	1.499	444	406.2
1m (1_1)	73	95	0.356	0.463	128	108.56
1.5m	32	38	0.153	0.182	55	48.73
2m	18	23	0.086	0.110	31	27.35

Table 6-4 a. One Lamp, Fixed Point Irradiance Results, 50cm steps

Distance	Average [RAW]	Maximum [RAW]	Average [V]	Maximum [V]	Avg. Irradiance [μW/cm²]	Expected Irradiance [μW/cm²]
0.1m	1022	1023	4.987	4.992	1795	[saturation]
0.2m	996	1023	4.86	4.992	1749	1815
0.3m	703	713	3.43	3.479	1234	979
0.4m	390	436	1.9	2.12	684	594
0.5m	253	307	1.234	1.498	444	396
0.6m	217	222	1.059	1.083	381	275
0.7m	160	165	0.78	0.805	280	198
0.8m	125	129	0.61	0.629	219	154
0.9m	100	105	0.488	0.512	175	121
1m	73	95	0.356	0.463	128	108

Table 6-4 b. One Lamp, Fixed Point Irradiance Results, 10cm steps

We note that the average irradiance is not exactly the same as the expected irradiance. This is because the calculated irradiance is in a perfect scenario while our tests were conducted in a real-world scenario that also contains noise. The main sources of noise to the UV detector are:
- Shot noise (Poisson noise) from electrical charges, dark current etc.
- Feedback noise of the UV detector
- Thermal (Johnson) noise
- Period noise associated with the current flow

- Preamplifier circuit and voltage noise [23].

Next, we take the test results data and plot them on the chart shown in Figure 6-7.
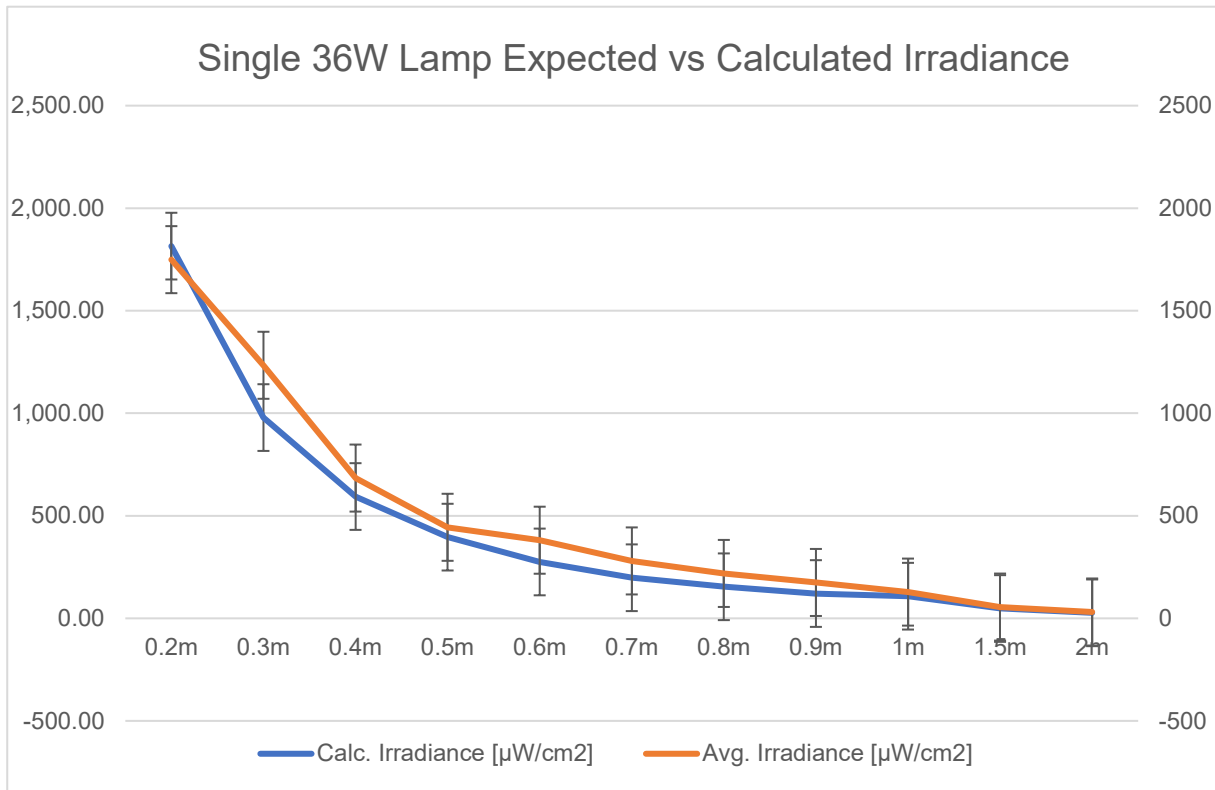
Figure 6-7 One Lamp, Fixed Point Chart Results

We can immediately note that the irradiance values are not linearly to the distance between the UV detector and the UV lamp, but rather logarithmical. This is achieved because of the inverse-square law stating that the specified light radiation is inversely proportional to the squared distance from the emitter (the UV-C lamp) to the receiver (the UV-C detector) as illustrated in Figure 6-8.
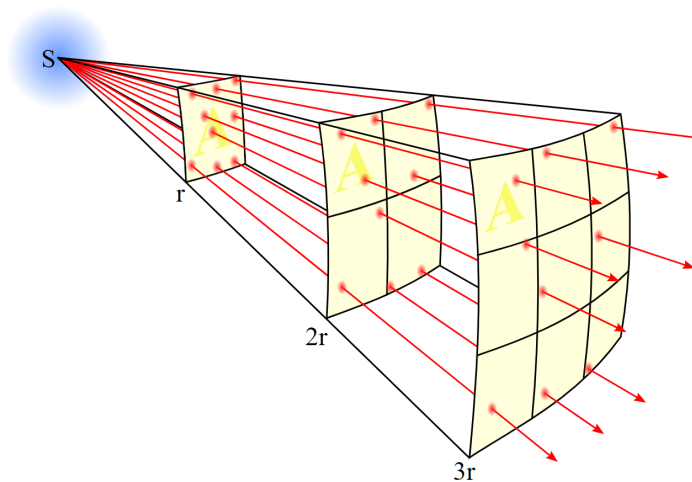
Figure 6-8. Inverse-Square Law: flux density lines

The formula (6-4) states this relationship between distance and intensity and the intensity resulted from this shown in formula (6-5) where P is the source power in watts and r is half the distance between our detector and the light source.

$$intensity \approx \frac{1}{distance^2} \qquad (6\text{-}4)$$

$$I = \frac{P}{A} = \frac{P}{4\pi r^2} \qquad (6\text{-}5)$$

Applying the general inverse-square law formula (6-4) to light irradiance we get the irradiance to distance formula shown in (6-6) where I is the irradiance in W/m², d is distance and k is the product of irradiance and the square of the distance

$$I = \frac{k}{d^2} \qquad (6\text{-}6)$$

When taking the aforementioned formula and plotting it in a chart we get results as shown in Figure 6-9 taken from [24] and we note that the general line is similar to the chart resulted from our test data.
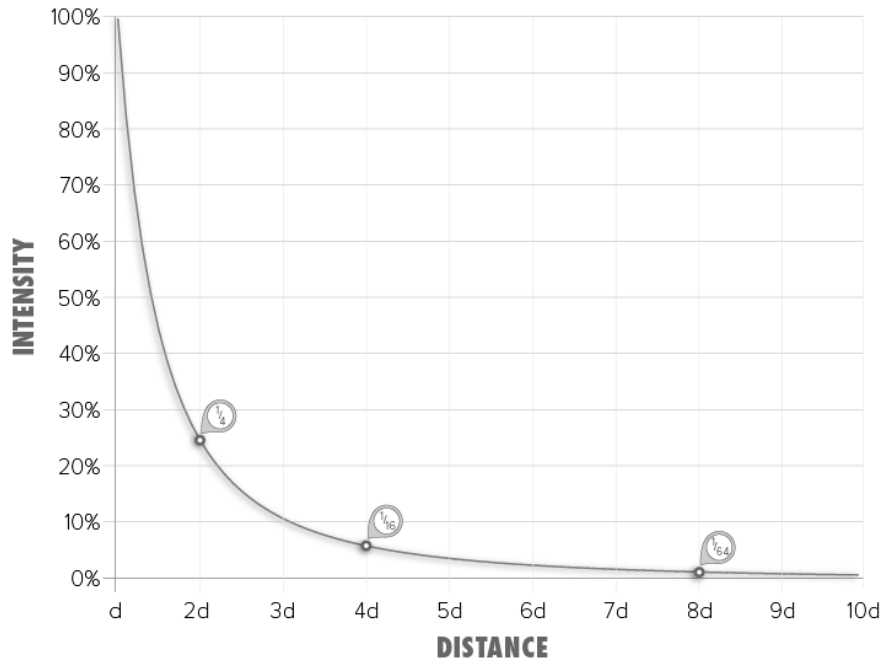

Figure 6-9. Change in light intensity over distance

When applying the (6-5) inverse-square law and compare it to our readings we note that our readings do indeed follow this rule as can be seen from TABLE

Distance	Measured Irradiance [μW/cm²]	Expected Irradiance [μW/cm²]
0.5 meters	444	458.5
1 meter	128	114.5 [110]
1.5 meters	55	50.9
2 meters	31	28.6

Table 6-5. Measured vs. Expected Irradiance

The sensor data, the average non-zero, and the maximum values were taken and computed on a series of 5600 readings from the sensor over a period of 392 seconds. Plotting all the raw sensor data into a chart we get the results shown in Figure 6-10.a for readings from a distance of 0.5 meters and Figure 6-10.b for readings from a distance of 1 meter. It can be noted from the charts that the sensor values follow a 6th degree polynomial function on both cases, from 0.5 meters and from 1 meter. We also note that the sensor values will drastically increase in the first 100 seconds of measurements and, after that, in some cases the values continue to rise almost linearly. This can happen because of wavelength interference,
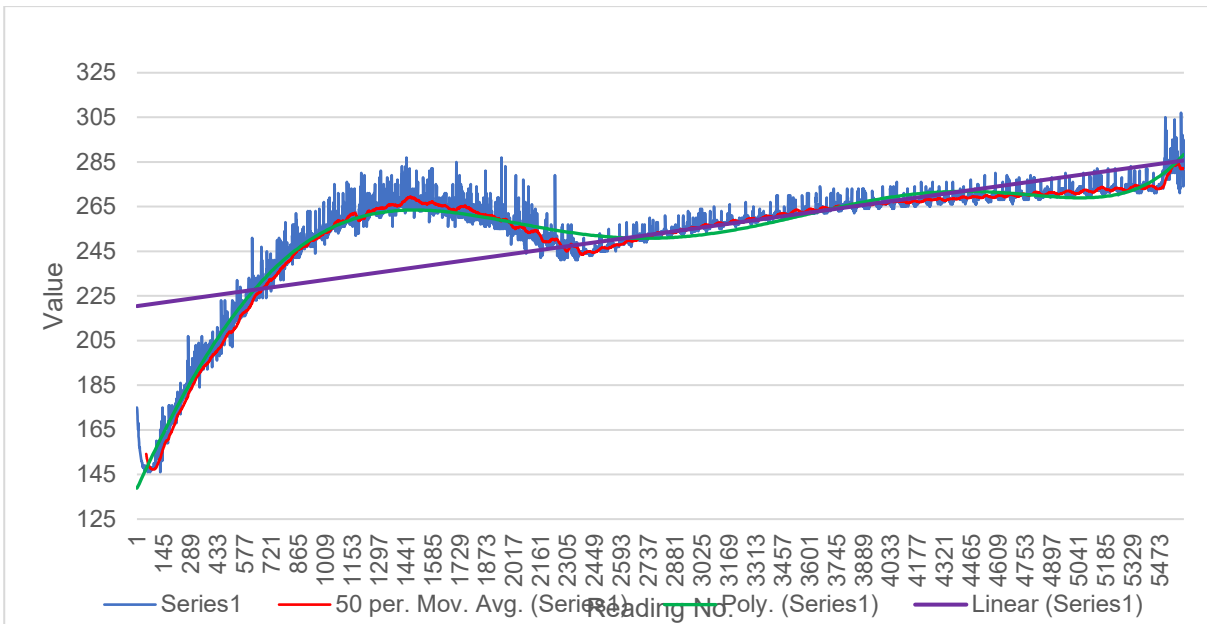
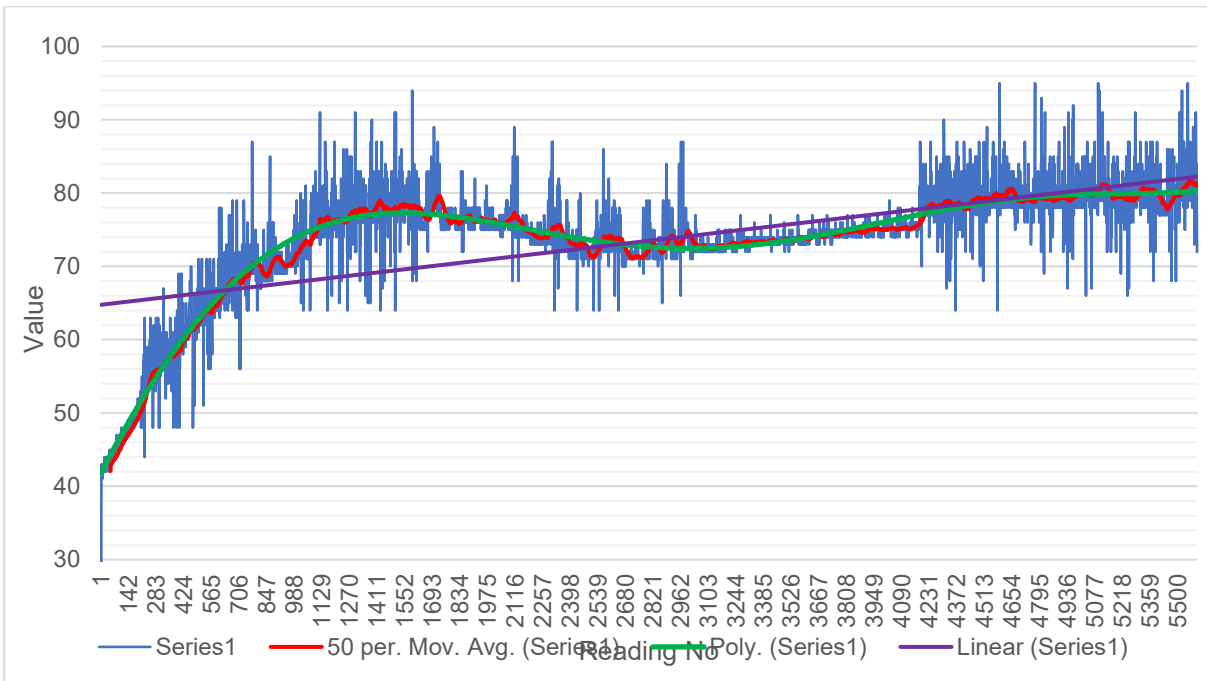Figure 6-10.a Raw Sensor values from 0.5 meters

Figure 6-10.b Raw Sensor Values from 1 meter

At the start of the acquisition process the UV-C sources are turned off. After approximately 10s, the UV-C sources are activated. Note the sudden rise in the sensor module response, then an evolution towards values which settle to averages of approximately 329mV or 118 µW/cm2.

42
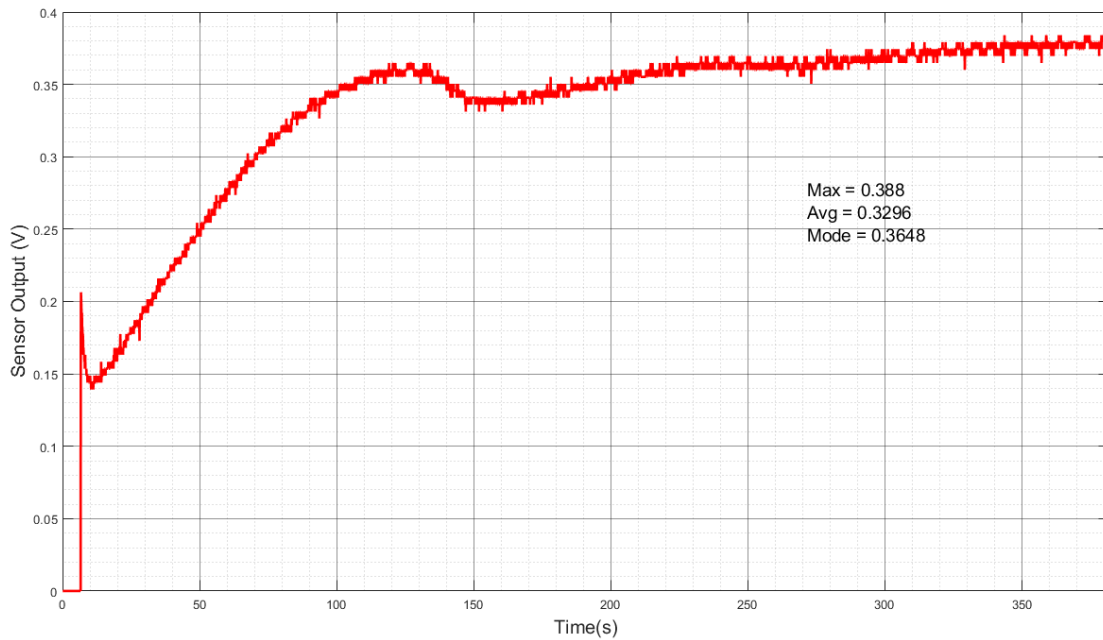
Figure 6-11. 1x36W Lamp Results Evolution

The following values are recorded for the last 190s of exposure time. We have estimated that after approximately 200s, the irradiance levels remain in a constant regime. In Figure 6-12 histogram evaluation of 1x36W lamp is shown.
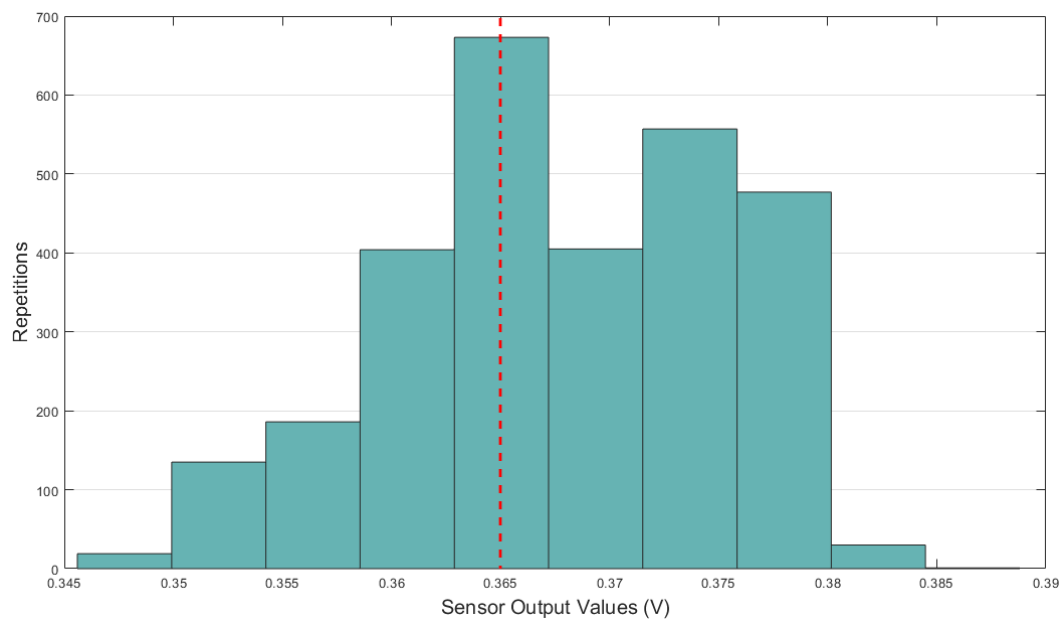
Figure 6-12. 1x36W Lamp Histogram Evaluation

In Figure 6-13.a one 36W lamp compared to two 36W lamps in Figure 6-13.b ensemble irradiance characteristics in relation with the measurement distance. The sensor module presents a maximum signal output at approximately 95% of the supply voltage. Assuming the supply voltage is ideal at 5V, the maximum accurate value returned by the C6 should be around 4.75V. Our datasets, at 0.2m and less, enters straight into the saturation zone of the sensor as expected. The 0.4m data sets achieve a peak of over 2.1V but stabilizes at an average of 2.038V as the dashed red line shows after approximately 200 seconds. Thus, the consistency of this datasets must be evaluated. The other datasets present good stability since they have been recorded after the initial warm-up period of the UV-C source.

43
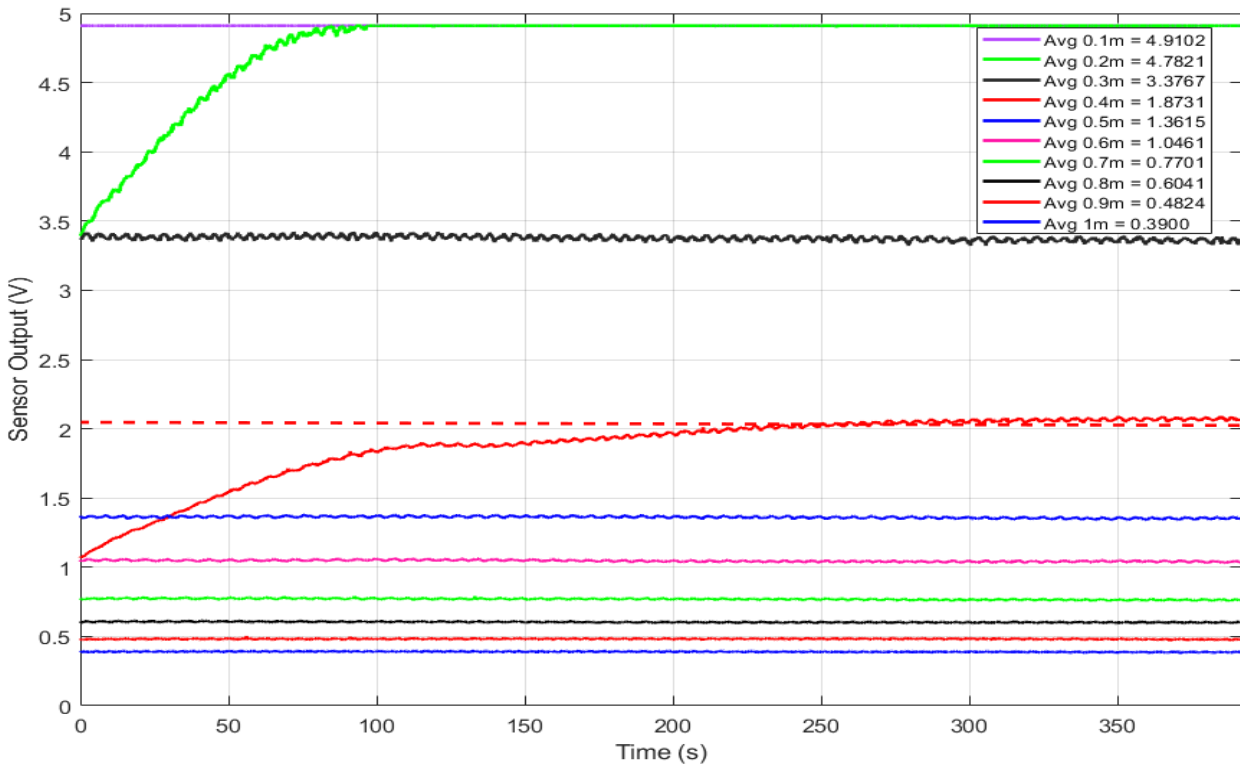
Figure 6-13.a 1x36W Distance Intensity Measurements
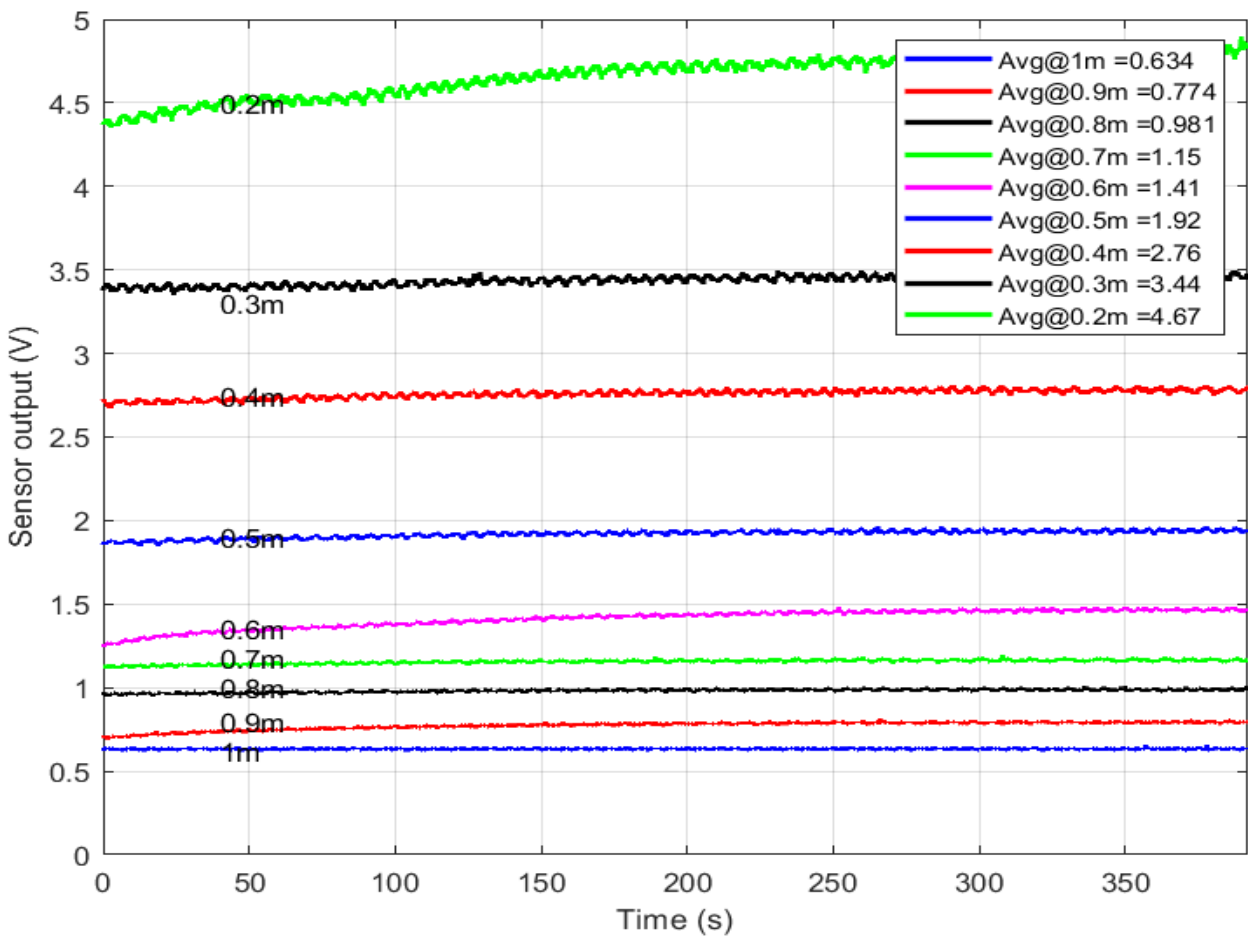
Figure 6-13.b 2x36W Distance Intensity Measurements

In our 3rd testing scenario, we are using two 36W UV-C lamps with a distance between them of approximately 7 cm as shown in Figure 6-14. The lamps are identical to the one used in the 2nd test, but we are using two of them. The platform's head will move in this scenario resulting a 2D grid array.
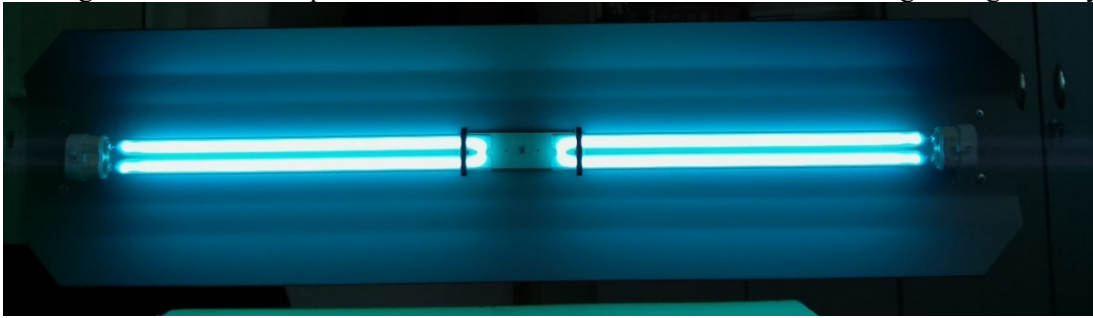
Figure 6-14. Two 36W lamps test environment

When using two lamps instead of a single one, interference occurs between the two lamp's wavelength. Because the wavelength of the light sources is identical (253.7nm), the resulting light waves are coherent but not perfect. Two light sources are coherent when they maintain a constant phase difference between them or, as long as the amount by which they are out of phase is constant over time as shown in Figure 6-15 from [25].
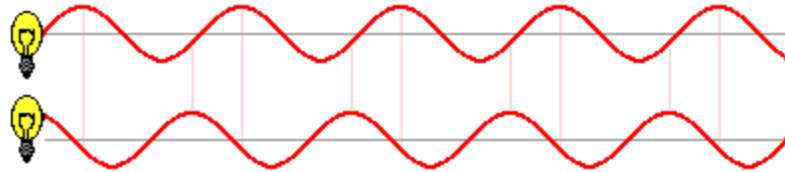
Figure 6-15. Coherent Light Sources

Because the light waves reach the UV detector at different angles, we cannot predict or accurately compute the intensity of both light sources as a whole. Interference and overlapping of plane waves will occur as shown in Figure 6-16.
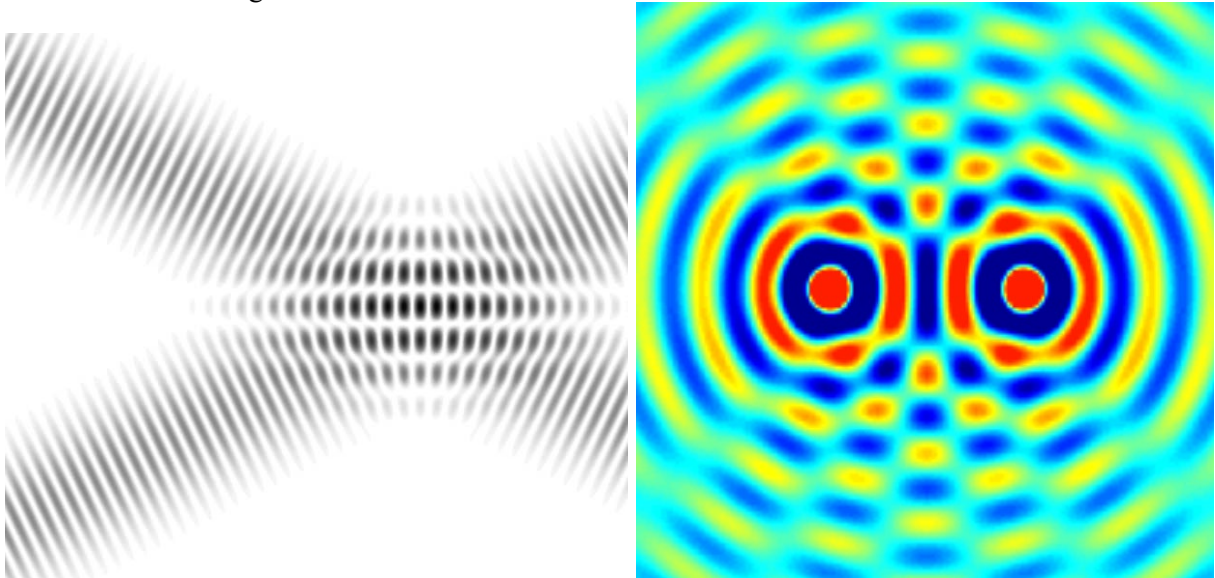
Figure 6-16. Overlapping wave planes

Continuing with our 3rd set of tests, multiple measurements have been made from distances of 0.5 meters, 1 meter, 1.5 meters and 2 meters. In the same manner as the first battery of tests, the head supporting the camera and the UV detector will move in order to create a 2D matrix image such as the one showed in Figure 6-17 and corresponding values shown in Table 6-5. Tests were conducted with a reference voltage of 5V.
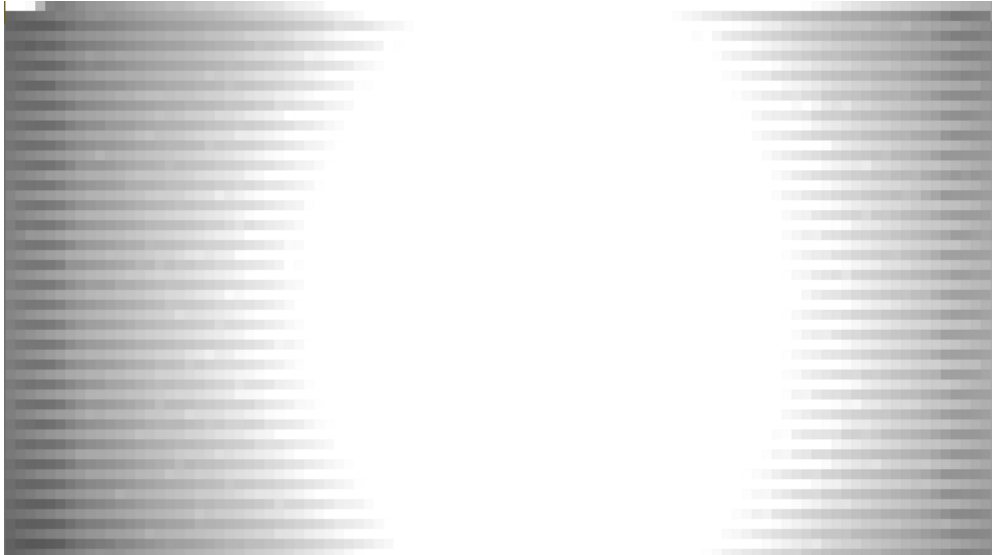
Figure 6-17. Two lamps, 2D Matrix Results, 0.5m

Because the sensor has a reference voltage of 5V this time, we get a resolution of 0.0048V/division.

Distance	Average [RAW]	Maximum [RAW]	Average [V]	Maximum [V]	Avg. Irradiance [μW/cm²]	Max Irradiance [μW/cm²]
0.5m	249	397	1.215	1.938	437.4	697.7
1m	84	140	0.41	0.683	147.6	245.9

Table 6-6. Two Lamps, 2D Matrix Results

We can see when comparing the results from the 2nd test to the results from the 3rd test that, when measuring on two UV sources, the final irradiance will not double as one would guess.

As a reference and comparison between the fixed-point measurement and the 2D matrix, sensor data from the 3rd test is shown in Figure 6-18. It can be noted from the chart that the values of the detector do not follow a linear progression but rather oscillates up and down, when the moving head is pointing away from the UV emitter, we have lower values, and when the moving head is pointing straight to the emitter, we have higher values, depending on the irradiance intensity with a peak value close to the center of the chart where the UV lamps are.
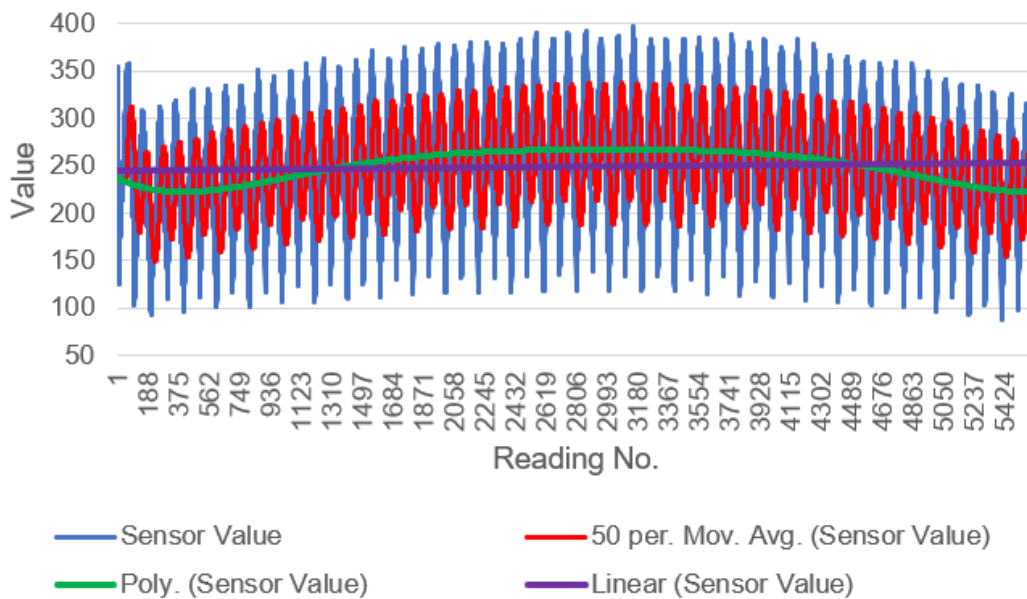
Figure 6-18. Two 36W lamps, 2D matrix results from 0.5m distance

7. Conclusions

In conclusion, the project was a great success. I was able to design, implement and create the robot platform that can be controlled from a safe distance in various (some dangerous) areas without the operator being in close vicinity.

The UV tests were also a big success, I was able to better understand how light, specifically ultraviolet light behaves and where and how exactly is UV light used, such as in disinfecting medical areas, food storages, water cleaning etc.

The robot platform has proven it is capable of conducting this type of tests in remote areas without human presence.

7.1. Achievements

The project has been a great learning experience for me, both from a software and hardware point of view. While working on the project, the biggest problems I came across was having stable video streaming at higher distances. Another setback in the project's development was being able to run all six motors without interfering or drawing too much power from the microcontroller and the wireless chip.

7.2. Future Work

The current state of the project can always be improved and I already have a few ideas in mind. The first thing I would improve is a close cover for the platform, right now all the wires are exposed and there is the risk that, if handled unproperly, some wires might pop-out of their respective pins and disconnecting. While being in the subject of lose wires, a custom-made PCB could be made in order to have better connectivity between the project's parts such as the one shown in Figure 7-1. This PCB was made prior to acquiring the MC6C controller and is also missing the 5V voltage regulator but a new one that contains everything currently on the platform can be made.
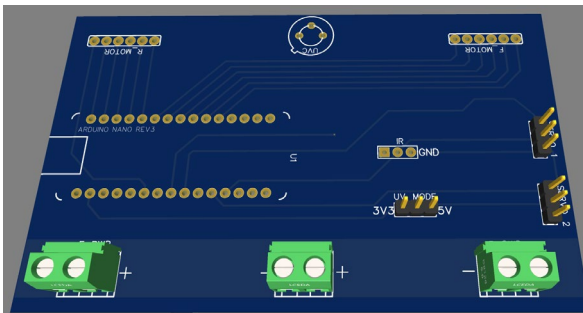
Figure 7-1.a Simulated 3D PCB   Figure 7-1.b Real PCB
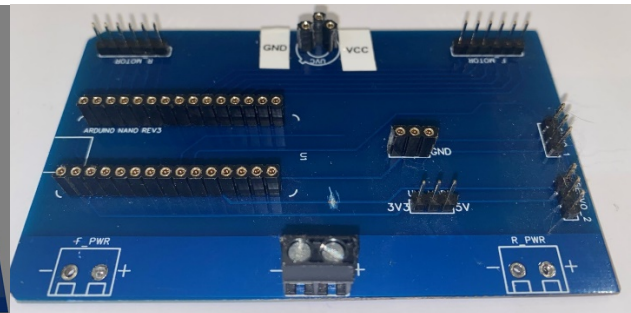
Another major update the platform could receive is a better video transmission system over larger distance. Our cameras can transmit up to tens of meters from the receiver (this drastically decreases based on environment, interference, obstacles etc.) because it uses a simple 2.4Ghz wireless connection. Systems that overcome this problem already exists such as FPV (First Person View) systems as shown in Figure 7-2.a. These types of systems usually use the 5.8Ghz spectrum and will utilize a larger band in order to have less interference. The FPV screen shown in Figure 7-2.a also requires a compatible FPV transmitter such as the one shown in Figure 7-2.b. Those systems are quite expensive but they can achieve transmission distances of up to 150 meters with obstacles in this particular case. There are even newer technologies such as the OcuSync 3.0 which is a proprietary state of the art technology from DJI made for drones and can achieve distances of up to 12km without any loss in quality and a delay of under 150 milliseconds.

In the near future, the following specific updates are planned:
- Remote specific updates:
  - Real-time generation of the matrix
  - Return-to-Home (RTH) – the robot will return to the same location it was started

- o Better video stream stability
- o Remote Fan control

- Platform specific updates:
  - o Bigger battery for driving the motors
  - o Enclosure
  - o Custom-made PCB
  - o Merging of two batteries, we'll be left with one big battery that powers everything.
  - o Bigger vertical motor (similar to the horizontal one).
  - o Smaller motor drivers.

Figure 7-2.a FlySight FPV Receiver   Figure 7-2.b FPV Transmitter

The motor drivers that are currently used in the project are quite big and not so efficient. Those can be replaced with newer and smaller drivers. Small SMD drivers that do not require any external circuits or heatsinks already exists and can be mounted directly on the custom-made PCB for minimal wiring allowing for a clean look of the project and a smaller form-factor but also less weight.

Currently there are two different batteries that will power the robot. One for the circuits and servo motors and one for the driving motors. Those can be replaced with a single battery after some modifications have been made to the platform.

There is currently no way of telling when the batteries will run out of power. A voltage indicator can be added in order to remotely control the battery state.

A battery charger would be a necessary addition to the robot. Currently, when the batteries need to be recharged, the respective battery is detached from the platform and connected to a charging station. With a single battery and a charger port will make charging the batteries much easier.

REFERENCES

[1]   J. Paul Chen et al., "Ultraviolet Radiation for Disinfection", *Advanced Physicochemical Treatment Processes* Vol 4, 317-366

[2]   Memarzadeh Farhad et al. "Applications of ultraviolet germicidal irradiation disinfection in health care facilities: effective adjunct, but not stand-alone technology." *American journal of infection control* (2010) 13:24

[3]   Wan-Sik Won et al., "UV-LEDs for the Disinfection and Bio-Sensing Applications", International Journal of Precision Engineering and Manufacturing Vol. 19, No. 12, pp. 1901-1915

[4]   Francisco A. Juarez-Leon et al. "Design and Implementation of a Germicidal UVC-LED Lamp", *Access IEEE*, vol. 8, pp. 196951-196962, 2020

[5]   T. Mathebula, F. W. Leuschner and S. P. Chowdhury, "The Use of UVC-LEDs for the Disinfection of Mycobacterium Tuberculosis", *IEEE PES/IAS PowerAfrica*, 2018, pp. 739-74

[6]   Jingyun FANG et al., "Jingyun FANGE. coli and bacteriophage MS2 disinfection by UV, ozone and the combined UV and ozone processes", Front. Environ. Sci. Eng. 2014

[7]   Reisz E, Schmidt W, Schuchmann H P, von Sonntag C. Photolysis of ozone in aqueous solutions in the presence of tertiary butanol. Environmental Science & Technology, 2003, 37(9): 1941–1948

[8]   Weihs P., Schmalwieser A.W., Schauberger G. (2012) *UV Effects on Living Organisms*, Meyers R.A. Encyclopedia of Sustainability Science and Technology. Springer, New York

[9]   J.M. Boyce, "Modern technologies for improving cleaning and disinfection of environmental surfaces in hospitals", Journal Antimicrobial Resistance and Infection Control, vol. 5, no. 10, pp. 1-10, April 2016.

[10]   J.H. Yang, U.I. Wu, H.M. Tai, and W.H. Sheng, "Effectiveness of an ultraviolet-C disinfection system for reduction of healthcare associated pathogens", Journal of Microbiology, Immunology and Infection, vol. 52, no. 3, pp. 487-493, June 2019.

[11]   C. Rock, B.A. Small and K.A. Thom, "Innovative Methods of Hospital Disinfection in Prevention of Healthcare-Associated Infections", Journal New Technologies and Advances in Infections Prevention - Current Treatment Options in Infectious Diseases, vol. 10, pp. 65-77, February 2018.

[12]   W.J. Kowalski, William P. Bahnfleth, "Effective UVGI System Design Through Improved Modeling" ….

[13]   "SOLVE II Science Implementation", *NASA*, 2003, Available: https://cloud1.arc.nasa.gov/solveII/implement.html (Accessed May, 2021)

[14]   "Ultraviolet disinfection guidance manual for the final long term 2 enhanced surface water treatment rule", Washington, DC: *United States Environmental Protection Agency*, 2011.

[15]   Messina Gabriele et al., "A new UV-LED device for automatic disinfection of stethoscope membranes". *American Journal of Infection Control. Elsevier*. 43 (10), 2015

[16]   Qualcomm Technologies, "AR3002 Single Chip Bluetooth v4.0 UART HCI Data Sheet", Sep. 2016

[17]   Microzone, "MC6C DataSheet", Accessed 2021

[18]   Roithner LaserTechnik Gmbh, "UVC Only Amplified SiC UV Detector" *UV-TIAMO-C6*, Available: http://www.roithner-laser.com/datasheets/pd/uv/uv-tiamoc6.pdf (Acces. May 26, 2021)

[19]   Paschotta, Dr. Rüdiger. *"Encyclopedia of Laser Physics and Technology - responsivity, photodetectors, photodiodes, sensitivity"*,
Available: https://www.rp-photonics.com/responsivity.html, (Accessed May, 2021)

[20]   Semiconductor Components Industries, "3.0 A, 15 V, Step−Down Switching Regulator", LM2576 Datasheet, January 2006

[21]   SCHEER (Scientific Committee on Health, Environmental and Emerging Risks), "Opinion on Biological effects of UV-C radiation relevant to health with particular reference to UVC lamps", February 2017

[22]   H.A.E. Keitz, "Light Calculations and Measurements", *An Introduction to the System of quantities and units in light-technology and to photometry",* March 1971

[23]   Arnold Daniels, *Field Guide to Infrared Systems, Detectors, and FPAs, Second Edition*, SPIE PRESS, 2010

[24]   *The Inverse-Square Law – There is just no escaping how light decays!,* Available: https://westernking.co.za/articles/the-inverse-square-law, Accessed April 2021

[25]   The Physics Classroom, *Mathematics of Two-Point Source Interference,* Available: https://www.physicsclassroom.com/Class/light/u12l3c.cfm#coherent (Accessed April 2021)

Rezumat in Limba Romana

Radiațiile ultraviolete există peste tot în jurul nostru, cu excepția UV-C și luminii cu unde mai mici. Lumina UV face parte din spectrul electromagnetic cu o lungime de undă cuprinsă între 100nm și 400nm [1]. Gama de lungimi de undă la dezinfectarea UV pe care urmează să lucrăm este de 220-280 nm (UV-C), în mod special 253,7nm, bacteriile având cea mai mare absorbtie a luminii de la 250nm la 265nm. Efectele biologice asupra supraexpunerii umane la radiațiile UV-C variază în funcție de lungimea de undă, energia fotonică și durata expunerii [2].

UV-C este clasificat ca si posibil cancerigen uman de către Programul Național de Toxicologie al SUA cu diverse consecințe în funcție de timpul de expunere, variind de la erupții ușoare în special în regiunea oculară și, în unele cazuri, poate duce chiar la cancer de piele și la moarte.

Lumina ultravioletă este invizibilă cu ochiul liber și este clasificată în patru părți: UV-A (315nm - 400nm), UV-B (280nm-315nm), UV-C (200nm-280nm) și Vacuum UV(100-200nm).

Dezinfectarea cu ultraviolete este o metodă de dezinfecție care a fost utilizată pe scară largă în echipamente de sterilizare utilizând UV-C (254nm). Ne propunem să demonstrăm pierderile și eficiența radiațiilor UV-C pe diferite distanțe fără interacțiune umana. Platforma propusă trebuie să se deplaseze în zona dorită, să identifice și să măsoare 253,7nm radiații, dacă există, produse de diverse surse. Platforma este controlată de la o distanță sigura și poate măsura intensitatea unui singur punct într-o perioadă scurtă de timp sau produce o matrice 2D care reprezintă dispersia radiației UV-C pe o perioadă mai lungă de timp.

Pentru a detecta și măsura de la distanță radiațiile ultraviolete fără a fi expusi radiațiilor, o platformă mobilă cu senzori urmează să fie creată după cum urmează. Platforma este capabilă să se deplaseze în toate direcțiile, înainte / înapoi, stânga / dreapta, dar și în diagonală cu capacitatea de a se roti pe loc. Această configurație a fost aleasă pentru a permite deplasarea ușoară a platformei în diferite zone și depășirea / evitarea obstacolelor. Senzorul pe care îl folosim împreună cu o cameră video sunt atașate la capul platformei. Capul este alcătuit din două servomotoare pentru a oferi o mișcare bidirecțională (sus/jos, stanga/dreapta). Această configurație permite utilizatorului să controleze individual camera montată pe două fără a muta platforma propriu-zisă și permite producerea unei matrice bidimensionale.

Sistemul propus a fost testat într-un spațiu expus la UV-C de la Universitatea Politehnica Timișoara, fără prezența umană. Pentru fiecare test, luăm un număr de 5600 de citiri cu detectorul UV-C, chiar si pentru citirile în punct fix. Astfel putem vedea evoluția, dacă există, a luminii de 253,7nm. În modul punct unic, măsurătorile sunt luate dintr-un singur punct fără a mișca capul. Numărul de măsurători este același ca în modul de măsurare a matricei 2D pentru consistență.

Pentru testele inițiale, la începutul procesului de achiziție, sursele UV-C sunt oprite. După aproximativ 10 secunde, sursele UV-C sunt activate. Există o creștere bruscă a răspunsului modulului senzor, apoi o evoluție către valori care se stabilizeaza la aproximativ 329mV sau 118 $\mu W/cm^2$ pentru o lampă și aproximativ 656mV sau 236 $\mu W/cm^2$ pentru două lămpi.

Prin inspecție, setul de date prezintă o precizie acceptabilă. Dacă luăm în considerare faptul că prin creșterea numărului de probe înregistrate, setul de date prezintă o distribuție normală, putem estima abateri standard de 2.7mV pentru o singură lampă de 36W și 4.7mV pentru două lămpi de 36W.

DECLARAŢIE DE AUTENTICITATE A LUCRĂRII
DE FINALIZARE A STUDIILOR [1]

Subsemnatul (a) _POP NICU-ŞERBAN_

_____ , legitimat (ă)

cu CI / BI seria _TZ_ nr. _522 300_ , CNP _1940429243823_

autorul lucrării _STUDY OF UV-C INTENSITY DISTRIBUTION USING_

THE TIAMO-C6 SENSOR

_____

elaborată în vederea susţinerii examenului de finalizare a studiilor de _MASTER_

INFORMATION TECHNOLOGY organizat de către Facultatea

DE AUTOMATICĂ ŞI CALCULATOARE din cadrul

Universităţii Politehnica Timişoara, sesiunea _IUNIE_ a anului

universitar _2020/2021_ , luând în considerare conţinutul art. 39 din

RODPI – UPT, declar pe proprie răspundere, că această lucrare este rezultatul propriei

activităţi intelectuale, nu conţine porţiuni plagiate, iar sursele bibliografice au fost

folosite cu respectarea legislaţiei romăne şi a convenţiilor internaţionale privind

drepturile de autor.

Timişoara,

Data   Semnătura

_01.06.2021_

---

[1] Declaraţia se completează „de mână" şi se inserează în lucrarea de finalizare a studiilor, la sfârşitul acesteia, ca parte integrantă.

Declaration of Authenticity

for

Bachelor Diploma or Master Dissertation Thesis*

I, the undersigned _POP NICU-ŞERBAN_____,

identified with ☑I.D./ ☐Passport, series _TZ___ no _522300_____,

issued by _SPCLEP TIMIŞOARA_____

from (country) _ROMANIA_____,

and personal identification number (PIN) _1940429243823_____,

author of the thesis" (title) _STUDY OF UV-C INTENSITY DISTRIBUTION_

_USING THE TIAMO-C6 SENSOR_____ "

conceived for taking the final exam in order to complete the ☐Bachelor/ ☑Master studies organized by the Faculty of _AUTOMATION AND COMPUTERS_____

from Politehnica University of Timisoara, in the ☑June/☐September/☐February session of the academic year 2020-2021, academic coordinator _RAUL CIPRIAN IONEL_____ taking into account the provision of art. 34 from the Regulation for Organizing and Conducting the Bachelor Diploma/ Master Dissertation Exams approved by the Senate Decision no. 109/14.05.2020 and knowing the fact that in case of subsequent finding of false statements, I will bear the administrative sanction provided by art. 146 of Law no. 1/2011 - the law on national education, namely the cancellation of the diploma, hereby declare on my own responsibility that:

- the work is the result of my own intellectual activity,
- the work does not contain texts, data or graphic elements from other works or from other sources without having cited these sources, including the situation in which the source is another work / other works of the undersigned,
- the bibliographic resources have been used in compliance with Romanian legislation and international conventions for copyright.,
- this work has not been presented before to another bachelor / diploma / dissertation examination committee.

Timişoara,

Date,   Signature

01.06.2021

_____

* The declaration will filled-in by hand and inserted in the Bachelor Diploma or Master Dissertation Thesis, at the end of the paper, as an integral part of the work.